A peptide of a type I toxin-antitoxin system induces *Helicobacter pylori* morphological transformation from spiral-shape to coccoids

Short title: *H. pylori* shape conversion induced by a TA toxin

Lamya EL MORTAJI[1], Alejandro TEJADA-ARRANZ[1,2], Aline RIFFLET[3], Ivo G BONECA[3], Gérard PEHAU-ARNAUDET [4], J. Pablo RADICELLA[5], Stéphanie MARSIN[5+] and Hilde DE REUSE[1*]

[1] Institut Pasteur, Département de Microbiologie, Unité Pathogenèse de *Helicobacter*, CNRS UMR 2001, 28 rue du Dr Roux 75724 PARIS Cedex 15 FRANCE.
[2] Université Paris Diderot, Sorbonne Paris Cité, Paris, France.
[3] Institut Pasteur, Département de Microbiologie, Unité Biologie et Génétique de la Paroi Bactérienne, CNRS UMR 2001, PARIS, FRANCE.
[4] Institut Pasteur, Imagopole, plate-forme de microscopie ultrastructurale, PARIS, FRANCE.
[5] Institute of Cellular and Molecular Radiobiology, Institut de Biologie François Jacob, CEA, Université de Paris, Université Paris-Saclay, Fontenay-aux-Roses, France.
[+] Current affiliation: I2BC/UMR 9198 CNRS- CEA -Université Paris-Saclay, Bat. 430, Orsay, FRANCE.

* Corresponding author: Hilde De Reuse (hdereuse@pasteur.fr)
Institut Pasteur, Unité Pathogenèse de *Helicobacter*
28, rue du Docteur Roux
75724 PARIS Cedex 15 FRANCE
Tel: +33 1 40 61 36 41

Summary

Toxin-antitoxin systems are found in many bacterial chromosomes and plasmids with roles ranging from plasmid stabilization to biofilm formation and persistence. In these systems, the expression/activity of the toxin is counteracted by an antitoxin, which in type I systems is an antisense-RNA. While the regulatory mechanisms of these systems are mostly well-defined, the toxins' biological activity and expression conditions are less understood. Here, these questions were investigated for a type I toxin-antitoxin system (AapA1-IsoA1) expressed from the chromosome of the human pathogen *Helicobacter pylori*. We show that expression of the AapA1 toxin in *H. pylori* causes growth arrest associated with rapid morphological transformation from spiral-shaped bacteria to round coccoid cells. Coccoids are observed in patients and during *in vitro* growth as a response to different stress conditions. The AapA1 toxin, first molecular effector of coccoids to be identified, targets *H. pylori* inner membrane without disrupting it, as visualized by Cryo-EM. The peptidoglycan composition of coccoids is modified with respect to spiral bacteria. No major changes in membrane potential or ATP concentration result from AapA1 expression, suggesting coccoid viability. Single-cell live microscopy tracking the shape conversion suggests a possible association of this process with cell elongation/division interference. Oxidative stress induces coccoid formation and is associated with repression of the antitoxin promoter and enhanced processing of its transcript, leading to an imbalance in favor of AapA1 toxin expression.

Our data support the hypothesis of viable coccoids with characteristics of dormant bacteria that might be important in *H. pylori* infections refractory to treatment.

51 **Significance Statement**

52 *Helicobacter pylori*, a gastric pathogen causing 800,000 deaths in the world annually,
53 is encountered both *in vitro* and in patients as spiral-shaped bacteria and as round
54 cells named coccoids. We discovered that the toxin from a chromosomal type I toxin-
55 antitoxin system is targeting *H. pylori* membrane and acting as an effector of *H. pylori*
56 morphological conversion to coccoids. We showed that these round cells maintain their
57 membrane integrity and metabolism, strongly suggesting that they are viable dormant
58 bacteria. Oxidative stress was identified as a signal inducing toxin expression and
59 coccoid formation. Our findings reveal new insights into a form of dormancy of this
60 bacterium that might be associated with *H. pylori* infections refractory to treatment.
61

62 **Introduction**

63 Toxin-antitoxin (TA) systems are small genetic elements that are widely distributed
64 on bacterial mobile genetic elements and among archaeal and bacterial genomes,
65 often in multiple copies (1–4). They code for a small stable toxic protein, designated
66 toxin, whose action or expression is counteracted by an unstable antitoxin molecule
67 that can either be an RNA or a protein (3, 5). Under conditions in which the toxins can
68 act, they target essential cellular processes or components (transcription, DNA
69 replication, translation, cell wall or membrane) resulting in growth arrest or cell death
70 (3, 5). The molecular mechanism of the toxins' activities and their regulation are often
71 known in detail while the biological function remains elusive. TA systems take part in
72 plasmid maintenance and protection from phage infection. Less is known on the
73 biological functions and targets of the chromosomally encoded TA systems. Some are
74 important for bacterial survival in their mammalian host (6) or biofilm formation (7).
75 There is accumulating evidence that upon stress conditions, some TA systems play a
76 role in the switch of actively growing bacteria to persisters or dormant cells (8–11).
77 Persister bacteria constitute a subpopulation that is metabolically active but slow-
78 growing and highly tolerant to antibiotics and stress conditions (11). Persistence is
79 considered as an important cause of recalcitrance of chronic bacterial infections to
80 therapy. However, stress-induced activation of TA-encoded toxins does not
81 necessarily cause persister formation (12) and it was more generally found that
82 decreased intracellular ATP concentration and/or low proton motive force (PMF) are
83 landmarks of persister formation (13, 14).

84 In the present work, we explored the role of TA systems in *Helicobacter pylori*, a
85 bacterium that colonizes the stomach of half of the human population worldwide and
86 causes the development of gastritis. In some cases, gastritis evolves into peptic ulcer
87 disease or gastric carcinoma that causes about 800,000 deaths in the world every year

88 (15, 16). This microaerophilic bacterium is unique in its capacity to persistently colonize
89 the stomach despite its extreme acidity and intense immune response (16). The
90 molecular mechanisms at the origin of this exceptional adaptation capacity of *H. pylori*
91 remain only partially understood. Their elucidation is crucial to understand *H. pylori*
92 virulence and to improve its eradication in patients with recurrent peptic ulcer disease.
93 *H. pylori* is a Gram-negative bacterium with a helical shape. Upon stress conditions
94 (antibiotics, aerobic growth) or prolonged culture, the shape of *H. pylori* progressively
95 evolves into a U-shape followed by a spherical form designated coccoid (17, 18). *H.*
96 *pylori* coccoids are non-culturable bacteria proposed to be dormant forms (18).
97 Recently, dormant non-culturable cells were associated with a deeper state of
98 dormancy as compared to persister cells (19).

99 *H. pylori* coccoids were observed in human gastric biopsies and, like spirals, adhere
100 to gastric epithelial cells (20). Despite numerous reports on coccoid forms of *H. pylori*,
101 no cellular effector of this conversion has been reported so far.

102 In type I TAs, the antitoxin is a small regulatory RNA inhibiting the synthesis of the
103 toxin by base pairing the toxin-encoding mRNA (3–5, 21, 22). Four families (A-B-C-D)
104 of conserved type I TA systems are expressed from the chromosome of *H. pylori*, only
105 the A family was studied as it is highly expressed and conserved among *H. pylori*
106 strains (23–25). For the A1 TA system, the detailed mechanism by which transcription
107 of the IsoA1 antitoxin RNA impairs AapA1 toxin synthesis by base pairing with its
108 primary transcript, ensuring both translation inhibition of the AapA1 active message
109 and leading to rapid degradation of the duplex by RNase III, has been recently
110 published (24, 25). The *H. pylori* type I toxins are typically small hydrophobic peptides
111 of 30-40 amino acids predicted to form alpha-helices (26). No clues on the mode of
112 action or the physiological role of these systems have been reported.

113 Here we show that the AapA1 toxin induces a rapid morphological transformation of
114 *H. pylori* from spirals to coccoids by targeting the inner membrane and probably
115 interfering with cell elongation and division. Furthermore, oxidative stress induces
116 coccoid formation and triggers imbalanced expression of the TA components in favor
117 of toxin production.
118

119 **Results**

120 **The AapA1 toxic peptide, expressed by the AapA1/IsoA1 TA system, triggers**
121 **rapid transformation of *H. pylori* into coccoids**

122 Recently, the study of the AapA1/IsoA1 TA system of *H. pylori* (**Fig. 1A**) showed
123 that expression of the AapA1 toxin (a 30 amino acids-long hydrophobic peptide) leads
124 to bacterial growth arrest (24). Given the genetic organization of the type I
125 AapA1/IsoA1 locus in B128 strain, we decided to investigate the mechanism
126 underlying the activity of AapA1 by using a strain in which AapA1 is under the control
127 of an inducible promoter. We thus transformed *H. pylori* strain B128 deleted of the
128 AapA1/IsoA1 chromosomal locus with each of the three plasmids constructed by
129 Arnion *et al.* (24) (**Fig. 1A**). The first, pA1-IsoA1, derived of the pILL2157 vector (27)
130 contains a functional TA locus in which the AapA1 gene is under the control of an IPTG
131 inducible promoter (24). In plasmid pA1, derived from this first construct, the antitoxin
132 IsoA1 promoter has been inactivated by point mutations that do not interfere with
133 transcription or translation of the AapA1 ORF (24). Derived from this second construct,
134 plasmid pA1* contains an additional mutation that inactivates the start codon of the
135 AapA1 peptide (24). Under our experimental conditions, we observed, in agreement
136 with data of (24), that addition of IPTG did not significantly influence the growth rate of
137 strains harboring pA1-IsoA1 or pA1*. In contrast, addition of the inducer causes a rapid
138 growth arrest of *H. pylori* with pA1 indicating a toxic effect of AapA1 expression (**Fig.**
139 **1B**). The growth arrest was accompanied by loss of culturability of more than 10^3-fold
140 8h after induction.

141 In parallel to growth, we investigated the consequences of AapA1 expression on *H.*
142 *pylori* morphology. Samples from bacterial cultures with these plasmids were grown in
143 the presence or absence of IPTG, stained with a membrane-specific dye, FM4-64, and
144 analyzed by fluorescence microscopy at 0h, 8h and 24h (**Fig. 1C**). *H. pylori* cells

145 expressing the wild-type AapA1/IsoA1 locus (pA1-IsoA1) or the pA1* mutated locus
146 present a classical helical rod-shaped phenotype upon IPTG exposure (**Fig. 1C**).
147 Under the same conditions, we observed that cells carrying the pA1 plasmid, and thus
148 expressing the AapA1 toxin exhibit a rapid morphological conversion to spherical cells
149 also known as coccoid forms (**Fig. 1C**). Using MicrobeJ (28) analysis of the phase
150 contrast images, we quantified the relative proportions of coccoids vs spiral bacteria
151 under each condition (**Fig. 1D**). When the toxin is expressed (pA1+IPTG), about half
152 of the cells have converted into coccoid as soon as 8h post-induction without further
153 changes at 24h post-induction. No bacterial lysis was detected even at 24h post-
154 induction. With strains carrying the pA1* plasmid, significant amounts of coccoids were
155 only observed after 64h of culture, similarly to the control wild type strain containing an
156 empty plasmid. These data show for the first time that the AapA1 toxin induces a fast
157 conversion of *H. pylori* cells from spiral-shaped to coccoid forms.
158
159 **Inner membrane targeting by the AapA1 toxin**
160 To investigate the mode of action of the AapA1 toxin, we first analyzed its subcellular
161 localization in *H. pylori* using a GFP reporter. A C-terminal fusion of the toxin with GFP
162 (A1-GFP) was introduced into B128 strain deleted of the chromosomal AapA1/IsoA1
163 module and expressed either from the chromosome under control of its native
164 promoter or from the IPTG-inducible promoter of vector pILL2157 (27) (**Fig. S1**). After
165 IPTG induction, the plasmidic fusion did not affect *H. pylori* growth indicating that a C-
166 terminal GFP fusion prevents the toxicity of the toxin. Attempts to construct N-terminal
167 tagged-AapA1 were unsuccessful.
168 Cellular fractionation was then performed on the strains, and the subcellular
169 localization of the fused toxin was analyzed by immunoblotting. **Figure 2A** shows that
170 the AapA1-GFP fusions expressed from the chromosome or from the plasmid are

171 almost exclusively present at the inner membrane of *H. pylori*. No A1-GFP peptide was
172 detected in the culture medium. Fluorescence microscopy of live bacteria after
173 induction of the AapA1-GFP fusion revealed a weak patchy pattern in the periphery of
174 the cell (**Fig. 2B**), different from a GFP-alone control cell (**Fig. S2**), and compatible
175 with membrane localization. This observation was confirmed by measuring the overlap
176 of the fluorescence intensity profiles of the toxin and TMA-DPH membrane dye
177 measured perpendicular to the length axis of *H. pylori* (**Fig. 2B**).
178 From these results, we conclude that the AapA1 toxin is specifically targeted to the
179 inner membrane of *H. pylori*.
180

181 **AapA1 toxin has a minor impact on *H. pylori* membrane potential and**
182 **intracellular ATP content**

183 Considering the membrane localization of the toxin, we hypothesized that AapA1
184 expression could affect the membrane potential and by consequence the ATP content
185 of the cells. To explore this possibility, *H. pylori* cells harboring pA1-IsoA1, pA1* or pA1
186 plasmids were taken at different culture time points (0, 8 and 24h), exposed to
187 MitoTracker Red CMXRos, a red-fluorescent dye whose accumulation inside live
188 bacteria depends upon membrane potential, and fluorescence of individual cells was
189 measured by flow cytometry. As a control, fluorescence was measured for the pA1*
190 strain treated with 3,5,3',4'-tetrachlorosalicylanilide (TCS), an effective *H. pylori*
191 protonophore (29). The TCS treatment causes a massive drop in fluorescence due to
192 dissipation of membrane potential (**Fig. 2C**, **Fig. S3**). We observed that, when the
193 AapA1 toxin is expressed in *H. pylori*, the membrane potential is maintained. Only a
194 weak drop was observed at 6h after induction that was slightly more pronounced at
195 24h (**Fig. 2C**).

196 Next, the ATP content of *H. pylori* strains carrying either pA1-IsoA1 or pA1 was
197 measured from total metabolites extracted at different culture time points and
198 quantified by a luciferase based-assay (**Fig. 2D**). After 6h of culture, IPTG induction
199 had a minor effect on cellular ATP content of both strains as compared to the drastic
200 consequences observed with the TCS control. At 6h post-induction, many pA1-
201 containing cells have already transformed into coccoids (see live imaging data below).
202 After 16h post-induction, in stationary phase, the overall ATP content strongly drops in
203 both strains and IPTG induction causes an additional weak decrease that is poorly
204 changed upon toxin expression by pA1 (**Fig. 2D).**
205 Taken together, these results show that the AapA1 toxin slightly perturbs the *H.*
206 *pylori* membrane potential with no major consequences on the cellular ATP content.
207 We conclude that dissipation of membrane potential is not the major cause of toxin-
208 induced bacterial growth arrest.
209
210 **Ultrastructural analysis of toxin-induced coccoids**
211 For the first time, cryo-electron microscopy (cryo-EM) was used to visualize *H. pylori*
212 coccoids in near-native states. Using this method, we compared exponentially growing
213 bacteria, toxin-induced coccoids and "aging coccoids" (70h growth) (**Fig. 3**). In
214 exponential phase, the characteristic helicoidal shape of *H. pylori* (strains B128 WT,
215 4h and pA1-IsoA1, 4-8h) was perfectly visible with a uniformly contrasted cytoplasm
216 surrounded by two dense layers of membranes. The periplasm of variable thickness
217 surrounding the cell is distinguishable as the low-density space between the inner and
218 outer membrane. Strains expressing the toxin (pA1 at 4-8h) have intact flagella and
219 are visible in two major morphotypes. In the first “U” shaped morphology, a round intact
220 outer membrane surrounds a bent intact inner membrane. The second morphotype
221 corresponds to round coccoids of a diameter of approximately 1µm, with visible

222 integrity of both membranes and a central uniformly stained dense cytoplasm. This
223 second morphotype is similar to that of aging coccoids from the WT strain (70h).
224 In conclusion, cryo-EM images revealed that the toxin-induced *H. pylori* coccoids
225 have no visible defect in membrane integrity and are ultrastructurally similar to "aging
226 coccoid" forms.
227
228 **Modification of peptidoglycan composition upon transformation of *H. pylori* into**
229 **coccoids**
230 Our data showed that the AapA1 toxin targets *H. pylori* inner membrane without
231 causing significant membrane potential collapse and without visible loss of integrity.
232 Therefore, we tested whether the toxin-induced cell shape transformation could be
233 associated with modifications in the cell wall and thus in peptidoglycan (PG)
234 composition. PG extracted from B128 WT strain in exponential (24h of culture) or
235 stationary phase (36h of culture) or after 72h growth ("aging coccoids") was compared
236 to PG extracted from the pA1-bearing strain either 8h or 24h after induction (toxin-
237 induced coccoids, 24h and 36h total culture time) and from the pA1* strain as a
238 negative control. Samples were digested with mutanolysin and subjected to HPLC/MS
239 analyses. The relative abundance of muropeptides in each sample was calculated
240 according to Glauner *et al.* (30) (**Table S1**). We found that the PG of B128 WT
241 stationary phase and "aging coccoids" as well as the pA1 induced coccoids present
242 enhanced amounts of GlcNAc-Mur*N*Ac-dipeptide (GM2) as compared to helical
243 exponential phase *H. pylori* and to the negative control with pA1*. This GM2 increase
244 seems to be at the expense of the GM3 muropeptides, whose amount is reduced in
245 "aging coccoids" and in pA1-induced bacteria where it reaches a minimal value 24h
246 post-induction. This shows that during the transition from exponentially growing spiral
247 bacteria to coccoids, the muropeptide composition undergoes important modifications

248 that are comparable for the toxin-induced coccoids and "aging coccoids". These
249 changes, compatible with a looser PG macromolecule, suggest that the coccoid
250 formation under these two conditions might be generated by similar mechanisms.
251

252 **Kinetics of the toxin-induced *H. pylori* morphological transformation assessed**
253 **by live cell imaging**

254 To progress in our understanding of the morphological conversion of *H. pylori*, we
255 monitored the entire process of *H. pylori* toxin-induced conversion by live cell time-
256 lapse microscopy under physiological microaerobic conditions in a temperature-
257 controlled chamber. The *H. pylori* B128 strain tested constitutively expressed
258 cytoplasmic GFP, was impaired in motility (by deletion of *flaA* encoding the major
259 flagellar protein) and carried the inducible toxin-expressing plasmid pA1. Individual live
260 *H. pylori* bacteria were monitored in agarose pads by both bright field and fluorescence
261 microscopy.

262 First, the general growth features of the strain between cell birth and its next division
263 were established on 61 bacteria in the absence of the IPTG inducer. Under these
264 conditions, statistics of the data collected showed that the strain has a mean doubling
265 time of 165 min (indicative of optimal growth conditions) with an initial bacterial length
266 of 1.9 µm after division and a maximum length prior to division of 3.2 µm (**Fig. S4**). In
267 a second round of experiments, the A1 toxin was induced by IPTG addition to the pad
268 and snapshots of the cells were taken at intervals of 10 min during 10h (**Fig. 4**). A total
269 number of 158 cells were analyzed from 2 independent experiments that gave
270 consistent results. Three representative movies can also be viewed in **Fig. S5**. During
271 the 10h of analysis, about 70% of bacteria showed visible cell shape morphological
272 transformations; these bacteria were further analyzed. To quantify the changes in
273 shape of individual *H. pylori* cells over time, we used the MicrobeJ software (28) and

274 applied circularity attributes to discriminate the populations. As illustrated in **Fig. 4**, a
275 circularity value of 0.7 defines the first steps of *H. pylori* cells bending that is followed
276 by quasi-round bacteria (circularity >0.8) and finally fully developed coccoids
277 (circularity >0.9).

278 The changes in circularity were measured for 110 individual bacteria over time. **Fig.**
279 **4** provides an overall view of the progressive rounding of the analyzed bacteria. The
280 kinetics of circularity changes reveal that the first step (>0.7) starts as early as at a
281 median of 150 min post-induction, which is very close to the doubling time of *H. pylori*
282 cells. Most interestingly, the length of bacteria just before they enter the first
283 morphological transformation (circularity >0.7) was 3.46 µm (±0,6), which is very close
284 to the maximum length we measured before *H. pylori* division. In addition, we observed
285 many examples of two bacteria that were dividing but not yet separated and from which
286 one out of the two underwent morphological transformation (see movies in **Fig. S5**).
287 This analysis gave us a dynamic picture of the morphological transformation of *H.*
288 *pylori.* Importantly, it suggests that the observed morphological transformation is likely
289 to be consecutive to a toxin-induced perturbation of cell elongation and division,
290 through a mechanism that is still to be defined.

291

292 **Toxin-antitoxin imbalanced expression upon oxidative stress**

293 We then searched for the physiological signal that could trigger the induction of the
294 AapA1 toxin expression in *H. pylori*. First, the respective activities of individual *aapA1*
295 and *IsoA1* promoters were measured with chromosomally expressed transcriptional
296 *lacZ* fusions (**Fig. S1**). Under normal growth conditions, ß-galactosidase activities
297 indicated that the antitoxin promoter has a 10-fold stronger activity than the toxin
298 promoter (**Fig. 5A**). This result is consistent with type I TA features where the antitoxin
299 RNA is strongly expressed (but highly labile) compared to the more stable toxin

300 transcript that is expressed at a lower level (8, 9, 22). The *lacZ* fusions were then used
301 to follow the activity of the two promoters during *H. pylori* growth and to search for
302 conditions relevant to *H. pylori* life-style that could lead to imbalanced expression of
303 the two promoters. Only a slight increase in activity of both promoters was observed
304 over time of growth (**Fig. 5A**). No significant differential expression of the promoters
305 was observed upon acid, antibiotic stress or during exposure to high nickel
306 concentrations (**Fig. S6**). In contrast, oxidative stress induced by hydrogen peroxide
307 (H_2O_2) resulted in a strong specific decrease in the *IsoA1* promoter activity while, at
308 the same concentration, the toxin promoter activity was marginally reduced (**Fig. 5B**).
309 Exposure to paraquat, another oxidative stress agent, resulted in a comparable strong
310 decrease of both promoters. The expression patterns and stability of the *aapA1* and
311 *isoA1* transcripts were then analyzed by Northern blot with total RNA extracted at
312 different time points after rifampicin addition. As shown in **Fig. 5C** and **Fig. S7**, the
313 *aapA1* transcript was detected as a 175 nucleotide-long band with an estimated half-
314 life of approx. 120min. In contrast, the 75 nt *isoA1* full length transcript declines much
315 faster, with an estimated 25min half-life, and the production of an approx. 50 nt short
316 processed form. Upon hydrogen peroxide exposure, the half-life of the AapA1
317 transcript was not significantly modified while we observed a more rapid depletion of
318 the full-length *IsoA1* transcript with an almost immediate accumulation of the
319 processed form (**Fig. 5C**). From three independent experiments, we quantified the
320 relative amounts of the transcripts under normal growth conditions versus H_2O_2
321 exposure during 120 min after rifampicin addition (**Fig. 5D**). No significant change was
322 observed for the *aapA1* transcript while H_2O_2 exposure resulted in a diminished half-
323 life of the *IsoA1* full length transcript and in an imbalanced ratio of *IsoA1* in favor of its
324 processed form (**Fig. 5D**). Taken together, these results show that H_2O_2 causes both
325 diminished *IsoA1* transcription and increased degradation of *IsoA1* full-length

326 transcript. These observations suggest that, by decreasing the amounts of antitoxin
327 transcript, exposure to oxidative stress favors translation of the AapA1 mRNA and thus
328 toxin production that ultimately leads to coccoid transition.
329
330 **Oxidative stress induction of coccoids: are class A Type I TA the only effectors?**
331 Since we established that oxidative stress results in imbalanced expression in favor
332 of the expression of the AapA1 toxin, we examined the consequences of exposure to
333 H_2O_2 on *H. pylori* morphology and viability (**Fig. S8**). Upon treatment with 2% H_2O_2 of
334 WT B128 strain, we measured a partial conversion to coccoids (around 25%) either
335 after 6h or 24h. Treatment with 5% H_2O_2 resulted in a rapid and massive transformation
336 (about 90% of cells) of this strain into coccoids after 6 or 24h without detectable cell
337 lysis (**Fig. S8A**). Strain B128 contains six class A type I TA systems (**Fig. S9**). To
338 assess their role, we constructed mutants carrying deletions of each of its active
339 AapA/IsoA TA loci, Δ*A1*, Δ*A3*, Δ*A4* (including deletion of both *A4-1* and *A4-2* tandem
340 systems), Δ*A5*, Δ*A6* or of the five loci collectively (Δ*5*) using a non-marked deletion
341 strategy (31). A locus corresponding to the position of the A2 locus in other *H. pylori*
342 strains was identified but its corresponding A2 ORF was inactive in strain B128. Under
343 normal conditions, the growth rate, culturability and kinetics of occurrence of coccoids
344 of the different mutants were comparable to that of the parental strain (**Fig. S8**). Most
345 interestingly, treatment of the Δ5 mutant with 2% H_2O_2 revealed minimal conversion
346 after 6h of treatment with only 10% of the cells identified as coccoids as compared to
347 25% coccoid conversion for the wild type B128 strain. After 24h treatment, about 40%
348 of the Δ5 cells were coccoids. Upon treatment with 5% H_2O_2, both WT and Δ5 mutant
349 strain displayed similar kinetics of conversion to coccoids (**Fig. S8A**). This suggests
350 that, in the Δ5 strain, there is a significant delay in oxidative stress-induced coccoid
351 formation.

352 We conclude that oxidative stress is triggering transformation into coccoids through
353 type I class A TA systems but that other effectors are able to eventually drive this
354 conversion. In some cases TA systems have been shown to play a role in persister
355 cell formation under stress conditions (8, 10). Therefore, the number of persisters after
356 exposure to hydrogen peroxide was measured for the ΔA1 and Δ5 mutants and
357 compared to the parental strain (**Fig. S8**). No significant difference was observed,
358 suggesting that, upon hydrogen peroxide stress, the class A TA systems are not
359 promoting viable persisters in *H. pylori*.
360

361 **Discussion**

362 Here we established that the expression of a small toxin from a toxin-antitoxin
363 system triggers rapid morphological transformation of the spiral-shaped *H. pylori*
364 bacterium into round coccoid cells. Transformation of spirals into coccoids has been
365 observed after extended *H. pylori* growth (>70h, "aging coccoids") or upon stress
366 conditions (17) but the process itself was poorly characterized. Here we found that the
367 morphological transformation starts as soon as 2.5h after toxin induction and that
368 around 50% and 70% of the bacterial population convert into round coccoids
369 depending on the conditions (liquid culture vs agar pads for the live imaging). In liquid
370 culture, the amount of coccoids is probably underestimated since the vast majority of
371 the cells had lost culturability suggesting that they are indeed entering the process of
372 dormancy. We consider that the amount of 70% coccoid conversion that we observe
373 by live microscopy is a more accurate value since in these experiments the shape
374 evolution of single cells was precisely followed.

375 The toxin (AapA1) is a small hydrophobic peptide of a type I TA system that we
376 showed here to target *H. pylori* inner membrane without being secreted. Toxins of type
377 I TA systems from other organisms such as *Escherichia coli*, *Bacillus subtilis* or
378 *Staphylococcus aureus* have been shown to localize to the inner membrane but there
379 are no reports on induction of major cell shape modifications (4, 21, 32, 33). The *E.*
380 *coli* TisB (34) and the *S. aureus* PepA1 and PepA2 (35, 36) toxins act by creating
381 membrane pores (similar to phage holins) thereby disrupting the membrane potential,
382 drastically impairing ATP synthesis and depending on the toxin concentration, either
383 leading to the formation of persisters or to cell death (9, 33). One notable exception is
384 the BsrG/SR4 Type I TA system of *B. subtilis* (32). The BsrG toxin was found to target
385 the membrane without causing destruction or affecting the Proton Motive Force (PMF)
386 but it rather directly interferes with the cell envelope biosynthesis, indirectly delocalizes

387 the cell wall synthesis machinery and ultimately triggers bacterial autolysis (32). There
388 are now two examples of type I TA hydrophobic toxins (BsrG and AapA1 reported
389 here) that do not act by permeabilizing the membrane and probably reflect a novel
390 mode of action for small peptidic toxins.

391 Using cryo-EM on *H. pylori*, we observed that toxin-induced *H. pylori* coccoids
392 present neither visible membrane disruption nor pores even 8h post toxin induction
393 and are ultrastructurally comparable to 70h-old "aging coccoids". In addition, the
394 membrane potential of coccoids was not dissipated. This is in contrast with a previous
395 study that reported a total loss of membrane potential in *H. pylori* "aging coccoids",
396 associated with a complete loss of membrane integrity (37). Unlike the effects of the
397 TisB toxin in *E. coli* (34), we found that the ATP content in our *H. pylori* toxin-induced
398 coccoids is marginally affected and drops only after prolonged culture, as is the case
399 for spiral-shaped cells (38).

400 Toxins expressed by TA systems cause growth arrest by interfering with conserved
401 vital cellular processes such as translation, division or PG synthesis (9, 33). In bacteria,
402 PG cell wall dictates cell shape. We found that coccoid transformation was
403 accompanied by changes in PG composition. Indeed, when compared to spirals,
404 coccoids have a three-fold increase in dipeptide monomers concomitant with a
405 tripeptide monomers reduction. These changes are comparable to those previously
406 reported for "aging" *H. pylori* coccoids (39) and were confirmed here. Our results point
407 to a reduction in the potential for generating new cross-bridges in the PG; this is
408 compatible with a looser PG macromolecule and could explain the morphological
409 transition to coccoids.

410 Live imaging analysis of the toxin-induced conversion of *H. pylori* spirals into
411 coccoids suggested that the AapA1 toxin could interfere with cell elongation and
412 division. In *E. coli*, the CbtA toxin of a type IV TA system was found to inhibit cell

413 division and cell elongation via direct and independent interactions with FtsZ and MreB
414 (40). More work is needed to identify the molecular target(s) of the AapA1 toxin.
415 Under normal conditions, as for all TA systems, the *IsoA1* antitoxin potently inhibits
416 the AapA1 toxin, by preventing its expression through a multilayered mechanism (24,
417 25). We searched for physiological conditions that could result in toxin expression. We
418 found that oxidative stress, generated by H_2O_2, causes a rapid and specific decline in
419 the levels of IsoA1 antitoxin full-length transcript by reducing both its promoter activity
420 and enhancing its degradation through a mechanism that remains to be precisely
421 defined. Imbalanced expression of the AapA1/IsoA1 system in favor of the toxin mRNA
422 should lead to toxin expression. Accordingly, we observed that H_2O_2 causes a rapid
423 conversion of *H. pylori* into coccoids resembling those induced by the AapA1 toxin.
424 Prolonged exposure to aerobic conditions was previously reported to lead to coccoid
425 formation, however, in that case these cells lost their membrane integrity (41).
426 Regulation of type I TA systems in response to stress has been observed in other
427 species. For the *bsrE*/SR5 type I system of *B. subtilis*, the SR5 antitoxin is affected by
428 pH, anoxia and iron limitation while the BsrE toxin is sensitive to temperature shock
429 and alkaline stress (42). In *S. aureus*, the SprA1/SprA1$_{AS}$ system is induced in
430 response to acidic or oxidative stresses (35) and the antitoxin RNAs of the SprG/SprF
431 systems are reduced upon oxidative stress exposure (43). In *E. coli*, several type I
432 toxins are induced by the SOS response (8), a system that does not exist in *H. pylori*.
433 The biological function of *H. pylori* coccoids is still a matter of debate. Coccoids are
434 observed in prolonged *in vitro* cultures and induced by stress conditions, mostly
435 aerobic, anaerobic culture or exposure to antibiotic or oxidative stress. However, these
436 reports are difficult to compare since no standard procedure was used and analysis
437 was most of the time performed after more than a week exposure to stress (17, 37,
438 44). *H. pylori* coccoids are non-culturable cells under standard laboratory growth

439 conditions. Our analysis of both toxin-induced and 70h "aging coccoids" are in favor of
440 their viability despite their “unculturability”. We argue that contradictory conclusions on
441 viability refer to “damaged” or so-called “fragmented” coccoid forms corresponding to
442 membrane-less bacteria in prolonged 5 days-old *H. pylori* cultures (37). In favor of
443 coccoid viability are previous reports showing that coccoids express virulence factors
444 (17) and are capable, like spirals, of binding to host cells and inducing cellular changes
445 (45). *H. pylori* coccoids were also visualized in human gastric biopsies (46), probably
446 as part of biofilms (44); however it cannot be excluded that they correspond to a
447 transverse view of a spiral bacterium. In mice, coccoids induce gastritis (47) and can
448 revert to colonizing spiral bacteria (48). Taken together, these observations suggest
449 that coccoids are “dormant” viable forms of *H. pylori* that recover during host infection
450 and might play a role in transmission or in treatment failure. In agreement with this
451 view, Chaput *et al.* (49) showed that coccoids present decreased activation of NF-κB
452 and might allow the bacterium to escape the host immune response.

453 We showed that *H. pylori* coccoids are induced by a class A type I TA toxin and by
454 oxidative stress probably through the imbalanced expression of TA systems. During
455 infection, *H. pylori* is indeed exposed to harsh oxidative stress as a consequence of
456 the chronic inflammation it generates (50). Deletion of the five “class A” Type I TA
457 clusters of *H. pylori* was found to delay the oxidative stress induction of coccoids but
458 did not preclude it nor did it change the number of persister cells. We concluded that
459 these toxins are probably not the only triggers of coccoid transformation and suggest
460 that the two other classes of chromosomally-encoded type I TA systems (B and C
461 representing 9 systems) might also be important.

462 Dormant/persister bacteria present enhanced tolerance to antibiotics and in some
463 cases, have been shown to be induced by TA systems (8, 10), although other
464 mechanisms resulting in lowered ATP content and/or lowered PMF are also associated

465 with their occurrence (13, 14). We hypothesize that TA-induced *H. pylori* coccoids are
466 dormant bacteria as defined in a recent consensus review (51). As previously proposed,
467 non-culturable cells and “classical” dormant bacteria are part of a shared “dormancy
468 continuum” (52). In our model, this continuum would depend on the intracellular toxin
469 concentration as already suggested (53).

470 Stress-induced morphological transformation of bacteria into non-culturable
471 coccoid-like cells has been reported in at least 85 bacterial species among which are
472 important bacterial pathogens such as *Campylobacter jejuni, Vibrio cholerae* or
473 *Salmonella typhimurium* (19). For these organisms, the inducing trigger and function
474 remains to be characterized. We postulate that these forms are dormant bacteria and
475 that our findings on *H. pylori* might be more generally relevant and play important roles
476 in recurrent and persistent bacterial infections.

477

478 **References**

479 1. Y. Yamaguchi, J.-H. Park, M. Inouye, Toxin-Antitoxin Systems in Bacteria and
480 Archaea. *Annu. Rev. Genet.* **45**, 61–79 (2011).
481 2. N. Goeders, L. Van Melderen, Toxin-Antitoxin Systems as Multilevel Interaction
482 Systems. *Toxins.* **6**, 304–324 (2014).
483 3. R. Page, W. Peti, Toxin-antitoxin systems in bacterial growth arrest and
484 persistence. *Nat Chem Biol* **12**, 208–214 (2016).
485 4. S. Brantl, P. Müller, Toxin-Antitoxin Systems in *Bacillus subtilis*. *Toxins.* **11**, 262
486 (2019).
487 5. Q. E. Yang, T. R. Walsh, Toxin–antitoxin systems and their role in disseminating
488 and maintaining antimicrobial resistance. *FEMS Microbiol. Rev.* **41**, 343–353
489 (2017).
490 6. S. Helaine, *et al.*, Internalization of *Salmonella* by macrophages induces
491 formation of nonreplicating persisters. *Science* **343**, 204–208 (2014).
492 7. X. Wang, *et al.*, Antitoxin MqsA helps mediate the bacterial general stress
493 response. *Nat Chem Biol* **7**, 359–366 (2011).
494 8. B. A. Berghoff, E. G. H. Wagner, RNA-based regulation in type I toxin–antitoxin
495 systems and its implication for bacterial persistence. *Curr. Genet.* **6**, 1011 (2017).
496 9. A. Harms, D. E. Brodersen, N. Mitarai, K. Gerdes, Toxins, targets, and triggers:
497 An overview of toxin-antitoxin biology. *Mol. Cell* **70**, 768-784 (2018).
498 10. S. Ronneau, S. Helaine, Clarifying the link between toxin–antitoxin modules and
499 bacterial persistence. *J. Mol. Biol.* **431**, 3462–3471 (2019).
500 11. B. Gollan, G. Grabe, C. Michaux, S. Helaine, Bacterial persisters and infection:
501 past, present, and progressing. *Annu. Rev. Microbiol.* **73**, 359–385 (2019).
502 12. F. Goormaghtigh, *et al.*, Reassessing the role of type II toxin-antitoxin systems
503 in formation of *Escherichia coli* Type II persister cells. *MBio* **9**, e00640-18 (2018).

504 13. Y. Shan, *et al.*, ATP-Dependent Persister Formation in *Escherichia coli*. *MBio* **8**,
505 e02267-16 (2017).
506 14. Y. Wang, *et al.*, Inactivation of TCA cycle enhances *Staphylococcus aureus*
507 persister cell formation in stationary phase. *Sci. Rep.* **8**, 10849 (2018).
508 15. Y. Yamaoka, Mechanisms of disease: *Helicobacter pylori* virulence factors. *Nat*
509 *Rev Gastroenterol Hepatol* **7**, 629–641 (2010).
510 16. M. Amieva, R. M. Peek Jr, Pathobiology of *Helicobacter pylori*–induced gastric
511 cancer. *Gastroenterol* **150**, 64–78 (2016).
512 17. M. F. Loke, C. G. Ng, Y. Vilashni, J. Lim, B. Ho, Understanding the dimorphic
513 lifestyles of human gastric pathogen *Helicobacter pylori* using the SWATH-
514 based proteomics approach. *Sci. Rep.* **6**, 26784 (2016).
515 18. V. I. Reshetnyak, T. M. Reshetnyak, Significance of dormant forms of
516 *Helicobacter pylori* in ulcerogenesis. *World J. Gastroenterol.* **23**, 4867–4878
517 (2017).
518 19. M. Ayrapetyan, T. Williams, J. D. Oliver, The relationship between the viable but
519 nonculturable state and antibiotic persister cells. *J. Bacteriol.* **200,** e00249-18
520 (2018).
521 20. H. J. Chun, *et al.*, Electron microscopic evaluation of adhesion of *Helicobacter*
522 *pylori* to the gastric epithelial cells in chronic gastritis. *Korean J. Intern. Med.* **17**,
523 45–50 (2002).
524 21. S. Brantl, N. Jahn, sRNAs in bacterial type I and type III toxin-antitoxin systems.
525 *FEMS Microbiol Rev.* **39**, 413–427 (2015).
526 22. S. Masachis, F. Darfeuille, Type I toxin-antitoxin systems: regulating toxin
527 expression via Shine-Dalgarno sequence sequestration and small RNA binding.
528 *Microbiol. Spectr.* **6** (2018).
529 23. C. M. Sharma, *et al.*, The primary transcriptome of the major human pathogen

530 *Helicobacter pylori*. *Nature* **464**, 250–255 (2010).
531 24. H. Arnion, *et al.*, Mechanistic insights into type I toxin antitoxin systems in
532 *Helicobacter pylori*: the importance of mRNA folding in controlling toxin
533 expression. *Nucleic Acids Res.* **45**, 4782–4795 (2017).
534 25. S. Masachis, *et al.*, A genetic selection reveals functional metastable structures
535 embedded in a toxin-encoding mRNA. *Elife* **8**, e47549 (2019).
536 26. D. N. Korkut, *et al.*, Structural insights into the AapA1 toxin of *Helicobacter pylori.*
537 *Biochim. Biophys. Acta - Gen. Subj.* **1864**, 129423 (2020).
538 27. I. G. Boneca, *et al.*, Development of inducible systems to engineer conditional
539 mutants of essential genes of *Helicobacter pylori*. *Appl. Environ. Microbiol.***74**,
540 2095–2102 (2008).
541 28. A. Ducret, E. M. Quardokus, Y. V Brun, MicrobeJ, a tool for high throughput
542 bacterial cell detection and quantitative analysis. *Nat. Microbiol.* **1**, 16077 (2016).
543 29. K. Stingl, K. Altendorf, E. P. Bakker, Acid survival of *Helicobacter pylor*i: how
544 does urease activity trigger cytoplasmic pH homeostasis ? *Trends in Microbiol.*
545 **10**, 70–74 (2002).
546 30. B. Glauner, Separation and quantification of muropeptides with high-
547 performance liquid chromatography. *Anal Biochem.* **172**, 451-464. (1988).
548 31. F. Fischer, *et al.*, A novel essential ABC transporter and the NixA permease are
549 the two sole nickel uptake systems of *Helicobacter pylori*. *PLoS Pathog* **12**,
550 e1006018 (2016).
551 32. N. Jahn, S. Brantl, H. Strahl, Against the mainstream: the membrane-associated
552 type I toxin BsrG from *Bacillus subtilis* interferes with cell envelope biosynthesis
553 without increasing membrane permeability. *Mol. Microbiol.* **98**, 651–666 (2015).
554 33. R. Brielle, M.-L. Pinel-Marie, B. Felden, Linking bacterial type I toxins with their
555 actions. *Curr. Opin. Microbiol.* **30**, 114–121 (2016).

556 34. C. Unoson, E. G. H. Wagner, A small SOS-induced toxin is targeted against the
557 inner membrane in *Escherichia coli*. *Mol. Microbiol.* **70**, 258–270 (2008).
558 35. N. Sayed, S. Nonin-Lecomte, S. Réty, B. Felden, Functional and structural
559 insights of a *Staphylococcus aureus* apoptotic-like membrane peptide from a
560 toxin-antitoxin module. *J. Biol. Chem.* **287**, 43454–43463 (2012).
561 36. N. Germain-Amiot, *et al.*, A novel Staphylococcus aureus *cis-trans* type I toxin-
562 antitoxin module with dual effects on bacteria and host cells. *Nucleic Acids Res.*
563 **47**, 1759–1773 (2019).
564 37. J. G. Kusters, M. M. Gerrits, J. A. Van Strijp, C. M. Vandenbroucke-Grauls,
565 Coccoid forms of *Helicobacter pylori* are the morphologic manifestation of cell
566 death. *Infect. Immun.* **65**, 3672–3679 (1997).
567 38. H. Enroth, *et al.*, *In Vitro* aging of *Helicobacter pylori*: changes in morphology,
568 intracellular composition and surface properties. *Helicobacter* **4**, 7–16 (1999).
569 39. K. Costa, *et al.*, The Morphological transition of *Helicobacter pylori* cells from
570 spiral to coccoid Is preceded by a substantial modification of the cell wall. *J.*
571 *Bacteriol* **181**, 3710–3715 (1999).
572 40. D. M. Heller, M. Tavag, A. Hochschild, CbtA toxin of *Escherichia coli* inhibits cell
573 division and cell elongation via direct and independent interactions with FtsZ and
574 MreB. *PLoS Genet* **13**, e1007007 (2017).
575 41. H. Zeng, G. Guo, X. H. Mao, W. De Tong, Q. M. Zou, Proteomic insights into
576 *Helicobacter pylori* coccoid forms under oxidative stress. *Curr. Microbiol.* **57**, 281
577 (2008).
578 42. P. Müller, *et al.*, A multistress responsive type I toxin-antitoxin system: bsrE/SR5
579 from the *B. subtilis* chromosome. *RNA Biol.* **13**, 511–523 (2016).
580 43. C. Riffaud, M.-L. Pinel-Marie, G. Pascreau, B. Felden, Functionality and cross-
581 regulation of the four SprG/SprF type I toxin-antitoxin systems in *Staphylococcus*

582 *aureus*. *Nucleic Acids Res.* **47**, 1740–1758 (2019).

583 44. L. Cellini, *Helicobacter pylori*: A chameleon-like approach to life. *World J.*
584 *Gastroenterol.* **20**, 5575–5582 (2014).

585 45. E. D. Segal, S. Falkow, L. S. Tompkins, *Helicobacter pylori* attachment to gastric
586 cells induces cytoskeletal rearrangements and tyrosine phosphorylation of host
587 cell proteins. *Proc. Natl. Acad. Sci. U. S. A.* **93**, 1259–1264 (1996).

588 46. N. S. Goldstein, Chronic inactive gastritis and coccoid *Helicobacter pylori* in
589 patients treated for gastroesophageal reflux disease or with *H pylori* eradication
590 therapy. *Am. J. Clin. Pathol.* **118**, 719–726 (2002).

591 47. S. Nagai, *et al.*, Role of Peyer's patches in the induction of *Helicobacter pylori*-
592 induced gastritis. *Proc. Natl. Acad. Sci. U. S. A.* **104**, 8971–8976 (2007).

593 48. L. Cellini, *et al.*, Coccoid *Helicobacter pylori* not culturable *in vitro* reverts in mice.
594 *Microbiol. Immunol.* **38**, 843–850 (1994).

595 49. C. Chaput, *et al.*, Role of AmiA in the morphological transition of *Helicobacter*
596 *pylori* and in immune escape. *PLoS Pathog.* **2**, e97 (2006).

597 50. L. D. Butcher, G. den Hartog, P. B. Ernst, S. E. Crowe, Oxidative stress resulting
598 from *Helicobacter pylori* infection contributes to gastric carcinogenesis. *Cell. Mol.*
599 *Gastroenterol. Hepatol.* **3**, 316–322 (2017).

600 51. N. Q. Balaban, *et al.*, Definitions and guidelines for research on antibiotic
601 persistence. *Nat. Rev. Microbiol.* **17**, 441–448 (2019).

602 52. M. Ayrapetyan, T. C. Williams, J. D. Oliver, Bridging the gap between viable but
603 non-culturable and antibiotic persistent bacteria. *Trends Microbiol* **23**, 7–13
604 (2015).

605 53. E. Rotem, *et al.*, Regulation of phenotypic variability by a threshold-based
606 mechanism underlies bacterial persistence. *Proc. Natl. Acad. Sci. U. S. A.* **107**,
607 12541–12546 (2010).

608 54. M. Farnbacher, *et al.*, Sequencing, annotation and comparative genome
609 analysis of the gerbil-adapted *Helicobacter pylori* strain B8. *BMC Genom.* **11**,335
610 (2010).
611 55. M. S. McClain, C. L. Shaffer, D. A. Israel, R. M. J. Peek, T. L. Cover, Genome
612 sequence analysis of *Helicobacter pylori* strains associated with gastric
613 ulceration and gastric cancer. *BMC Genom.* **10**,3 (2009).
614 56. A. W. Debowski, *et al.*, Xer-cise in *Helicobacter pylori*: one-step transformation
615 for the construction of markerless gene deletions. *Helicobacter* **17**, 435–443
616 (2012).
617 57. S. Kutter, *et al.*, Protein Subassemblies of the H*elicobacter pylori* Cag Type IV
618 secretion system revealed by localization and interaction studies. *J. Bacteriol.*
619 **190**, 2161–2171 (2008).
620 58. M. El Ghachi, *et al.*, Characterization of the elongasome core PBP2:MreC
621 complex of *Helicobacter pylori*. *Mol. Microbiol.* **82**, 68–86 (2011).
622 59. S. Skouloubris, A. Labigne, H. De Reuse, The AmiE aliphatic amidase and AmiF
623 formamidase of *Helicobacter pylori*: natural evolution of two enzyme paralogs.
624 *Mol. Microbiol.* **40**, 596–609 (2001).
625 60. C. Muller, *et al.*, Hierarchical regulation of the NikR-mediated nickel response in
626 *Helicobacter pylori*. *Nucleic Acids Res.* **39**, 7564–7575 (2011).
627 61. C. Corbinais, A. Mathieu, T. Kortulewski, J. P. Radicella, S. Marsin, Following
628 transforming DNA in *Helicobacter pylori* from uptake to expression. *Mol Microbiol*
629 **101**, 1039–1053 (2016).
630 62. J. H. Miller, *A short Course in Bacterial Genetics : A laboratory manual and*
631 *handbook for Escherichia coli and related bacteria. Cold Spring Harbor, N. Y*
632 (Cold Spring Harbor Laboratory, 1992).
633 63. D. Kühner, M. Stahl, D. D. Demircioglu, U. Bertsche, From cells to muropeptide

634 structures in 24h: Peptidoglycan mapping by UPLC-MS. *Sci. Rep.* **4**, 7494 (2014).

635

636

637

638 **Figure legends**

639 **Figure 1: Expression of the AapA1 toxin from the AapA1/IsoA1 TA system**
640 **induces growth arrest and transformation of *H. pylori* strain B128 into coccoids.**
641 **A) Genetic organization of AapA1/IsoA1 locus in *H. pylori* B128 strain with the**
642 **AapA1 transcript encoding the toxin and the *IsoA1* antitoxin RNA.** Below is the
643 representation of the inserts of the three plasmids used in this study (24), each derived
644 from the pILL2157 *E. coli/H. pylori* vector (27). These inserts are expressed under the
645 control of an IPTG inducible promoter. Plasmid pA1-IsoA1 expresses both the toxin
646 and the first 30 nucleotides of the *IsoA1* RNA antitoxin. In pA1, the promoter region of
647 IsoA1 was mutated without affecting the amino acid sequence of AapA1. Plasmid pA1*
648 was derived from pA1 and contained an additional mutation inactivating the start codon
649 of AapA1.

650 **B) Expression of the AapA1 toxin causes rapid growth arrest of *H. pylori*.** Growth
651 kinetics of *H. pylori* B128 strains carrying each of the three plasmids illustrated in panel
652 A, grown in the absence (black symbols) or in the presence of 1mM IPTG (empty
653 symbols) that was added at the time indicated by an arrow (16h).

654 **C) Expression of the AapA1 toxin induces transformation of *H. pylori* into**
655 **coccoids.** Microscopy analysis of the *H. pylori* B128 strains carrying each of the three
656 plasmids at 8h and 24h following IPTG addition or grown without IPTG. Phase-contrast
657 and fluorescence images are respectively represented on the upper and bottom panels.
658 *H. pylori* membranes were stained with the lipophilic dye FM4-64. The scale bar
659 corresponds to 2 μm.

660 **D) Quantification of the transformation of *H. pylori* into coccoids.** The proportion
661 of helical and coccoid bacteria under each condition was quantified with the phase
662 contrast images using the MicrobeJ software. The number of analyzed cells is
663 indicated for each condition.

664

665 **Figure 2: AapA1 toxin targets *H. pylori* inner membrane, weakly disturbs the**
666 **bacterial membrane potential and poorly affects intracellular ATP content.**
667 **A) AapA1 toxin localizes to the *H. pylori* inner membrane.** Western blot analysis of
668 total extracts (T), soluble extracts (SE), inner membrane (IM) and outer membrane
669 (OM) fractions prepared from *H. pylori* B128 strain expressing a GFP tagged-AapA1
670 toxin (pA1-GFP) expressed either from the chromosome or from a plasmid (pILL2157)
671 under the control of an IPTG-inducible promoter. Anti-NikR antibodies were used as a
672 control of the cytoplasmic fraction. The fractionation procedure was validated as shown
673 in **Fig. S2**.
674 **B) In live cells, AapA1-GFP localizes as discrete foci at the *H. pylori* membrane.**
675 Strain B128 expressing the AapA1-GPF fusion protein was analyzed on agarose pads
676 by fluorescence microscopy 6h after IPTG-induction. Membranes were stained with
677 TMA-DPH lipophilic dye. The membrane association of AapA1-GPF was quantified by
678 measuring the fluorescence intensity profile perpendicular to the length axis of *H. pylori*.
679 The graph shows the average fluorescence intensity profiles with standard deviation
680 (n=25). The fluorescence maxima separated by 0.5 µm correlate with the *H. pylori* cell
681 width.
682 **C) Analysis of the effects of the AapA1 toxin on *H. pylori* membrane potential.**
683 MitoTracker Red CMXRos, a membrane potential reactive dye was used to analyze
684 live *H. pylori* B128 strains expressing each of the three plasmids illustrated in **Fig. 1**.
685 Samples were taken at 0, 8 and 24h post-induction, stained with MitoTracker Red
686 CMXRos and the proton-motive force (PMF) was measured as the Mean Fluorescence
687 Intensity (MFI) by flow cytometry. The cell population distribution histograms are
688 presented in **Fig. S3**. Cells expressing the toxin (pA1) present a mild fluorescence
689 reduction after 8 or 24h of culture suggesting a weak disturbance of their membrane

690 potential. No changes were observed in cells containing either pA1-isoA1 or pA1*
691 plasmid. As a control, pA1*-bearing cells were treated with TCS (3,3',4',5-
692 Tetrachlorosalicylanilide), a protonophore active on *H. pylori*, resulting in a massive
693 loss of membrane potential. The experiment was performed three times. Error bars
694 represent the standard deviation, with * corresponding to $P < 0.05$, ** to $P < 0.01$, ***
695 to $P < 0.001$; **** to $P < 0.0001$, indicating that the mean values are significantly
696 different, and NS corresponding to non-significant, ($P > 0.05$).

697 **D) Measurement of intracellular ATP content.**

698 Intracellular ATP was extracted from B128 strains harboring pA1-IsoA1 or pA1 at 6 or
699 16h post-induction growth in the presence or absence of IPTG. B128 WT strain treated
700 with 500μM of TCS protonophore was used as a control of PMF dissipation. ATP
701 concentrations were determined using a luciferase-based assay (BacTiter-Glo™,
702 Promega). Results from 3 independent experiments performed in triplicates are shown.
703 Error bars represent the standard deviation, with * corresponding to $P < 0.05$, ** to P
704 < 0.01, *** to $P < 0.001$, **** to $P < 0.0001$, indicating that the mean values are
705 significantly different, and NS corresponding to non-significant, ($P > 0.05$).

706

707 **Figure 3: Ultrastructural analysis of toxin-induced coccoids and "aging"**
708 **coccoids by cryo-electron microscopy.**

709 Cryo-electron microscopy was used to compare "aging" coccoids (70 h-old cultures)
710 and exponentially growing B128 strains either WT or carrying plasmid pA1-IsoA1 or
711 pA1 grown for 4 or 8h in the presence of IPTG. Expression of the toxin results in the
712 formation of U-shaped bacteria at 4h and round coccoids cells at 8h with visible intact
713 bacterial cell envelope similar to the aging coccoids. Scale bar represents 1μm.

714

715 **Figure 4: Time-lapse microscopy of *H. pylori* conversion to coccoid upon toxin**
716 **expression.**
717 Live cell time lapse microscopy was used to record, during 10 hours every 10 min,
718 the morphological modifications of individual *H. pylori* B128 strain cells after IPTG-
719 induction of the AapA1 toxin. Representative movies of the transformation can be seen
720 in **Fig. S5**.
721 **A. Bright field and fluorescence images of two examples of these kinetics.**
722 Circularity (>0.7; >0.8; >0.9) of the bacteria was measured with the MicrobeJ software.
723 Scale bar represents 1µm.
724 **B. Quantification of the evolution of the formation of round *H. pylori* cells over**
725 **time after IPTG induction.**
726 The percentage of each type of bacterium was classified as a function of its circularity
727 (>0.7; >0.8; >0.9).
728
729 **Figure 5: Oxidative stress generated by hydrogen peroxide results in decreased**
730 **antitoxin promoter activity and promotes *IsoA1* transcript processing.**
731 **A) Activity of the AapA1 and IsoA1 promoters as a function of growth.**
732 β-galactosidase activities (expressed in Miller units) measured with *H. pylori* B128
733 strain carrying chromosomal P*aapA1-lacZ* and P*IsoA1-lacZ* fusions after 6, 24 and 48h
734 growth. Results from 3 independent experiments performed in duplicates are shown.
735 Error bars represent the standard deviation, with * corresponding to $P < 0.05$, and **
736 to $P < 0.01$, indicating that the mean values are significantly different, and NS indicating
737 that they are not significantly different ($P > 0.05$). The activity of the toxin fusion (*aapA1-*
738 *lacZ*) is about ten times that of the antitoxin fusion (*IsoA1-lacZ*) and the activity of both
739 promoters slightly increases as a function of growth.
740 **B) Oxidative stress generated by H_2O_2 decreases antitoxin promoter activity.**

741 β-galactosidase activities expressed by P*aapA1-lacZ* and P*IsoA1-lacZ* fusions were
742 measured after 6h treatment with oxidative stress generators, paraquat (5, 50 and 500
743 μM) and H_2O_2 (0.03 and 0.3%). β-galactosidase activities are presented as a ratio
744 (expressed in %) of activities measured with stress versus activities of untreated
745 samples. Hydrogen peroxide strongly decreases the expression of the P*IsoA1-lacZ*
746 fusion. Results from 3 independent experiments performed in duplicates are shown.
747 Error bars represent the standard deviation, with ** corresponding to $P < 0.01$ and ***
748 to $P < 0.001$, indicating that the mean values are significantly different, and NS
749 indicating that they are not significantly different ($P > 0.05$).

750 **C) Determination of AapA1 mRNA and IsoA1 RNA half-lives in *H. pylori* strain**
751 **B128 under normal conditions and upon hydrogen peroxide exposure.**

752 Northern blots of total RNA from B128 WT strain grown under normal conditions or
753 exposed to 1% hydrogen peroxide, extracted at the indicated times after addition of 80
754 μg/ml rifampicin. Five μg of RNA were loaded in each lane and the membranes were
755 probed with [γ-^{32}P] ATP-labeled oligonucleotides specific to the following RNAs, *aapA1*,
756 *IsoA1* and 5S rRNA as a loading control. In the presence of H_2O_2, the half-life of *IsoA1*
757 transcript is diminished in favor of the processed *IsoA1* form.

758 **D) Hydrogen peroxide promotes *IsoA1* transcript processing.**

759 Graphic representation of the effects of hydrogen peroxide exposure on the amounts
760 of *aapA1* and *IsoA1* transcripts as well as on *IsoA1* processing during 120 min after
761 rifampicin addition. The relative amounts of *aapA1* (upper graph) and full length (FL)
762 *IsoA1* (middle graph) RNAs versus 5S rRNA are shown. The lower graph presents the
763 relative amounts of the two forms of *IsoA1*, full length (FL) versus the processed form.
764 The results of 3 independent experiments are shown, error bars represent the standard
765 deviation analyzed by two-way ANOVA multiple comparisons.

Acknowledgments

This work was funded by the Agence National de la Recherche (ANR 09 BLAN 0287 01 and ANR 12 BSV5-0025-02), the Laboratoire d'Excellence IBEID (Integrative Biology of Emerging Infectious Diseases) Grant ANR-10-LABX-62-IBEID from the French government's Investissement d'Avenir program and the Pasteur-Weizmann Consortium of "The Roles of Noncoding RNAs in Regulation of Microbial Life Styles and Virulence". LEM was funded by a Roux fellowship of the Institut Pasteur and by a Carnot MI fellowship. ATA is part of the Pasteur Paris University (PPU) International PhD Program. This project has received funding from the European Union Horizon 2020 research and innovation program under the Marie Sklodowska-Curie grant agreement No 665807, and from the Institut Carnot Pasteur Microbes and Santé. AR was supported by post-doctoral fellowship from the Labex IBEID (10-LABX-62-IBEID). We also thank Janssen for financial support. We are grateful to F. Darfeuille, I. Iost and H. Arnion for the gift of plasmids and to W. Fischer for the gift of anti-AlpA antibodies. We also appreciate the expertise and help of A. Chery-Faleme, M. Fromont-Racine and A. Jacquier with Northern blotting, of R. Wheeler for peptidoglycan extraction, of Z. Baharoglu and I. Santecchia for flow cytometry and of A. Ducret for image analysis. We thank M. Denic and S. Kumar for comments on the manuscript and J. Berry for discussions. Finally, we thank M. Nilges and the Equipex CACSICE for providing the Falcon II direct detector.

788 **Material and Methods**

789

790 ***Bacterial strains and growth conditions***

791 The *H. pylori* strains used in this study (Suppl **Table S2**) were all derived of strain
792 B128 (54, 55). Plasmids (suppl **Table S3**) used to create or complement *H. pylori*
793 mutants were constructed and amplified using *E. coli* One-Shot TOP10 or DH5α
794 strains (Thermofisher). *H. pylori* strains were grown on Blood Agar Base 2 (Oxoid)
795 plates supplemented with 10% defibrinated horse blood and with the following
796 antibiotics-antifungal cocktail: amphotericin B 2.5 $\mu g.ml^{-1}$, polymyxin B 0.31 $\mu g.ml^{-1}$,
797 trimethoprim 6.25 $\mu g.ml^{-1}$ and vancomycin 12.5 $\mu g.ml^{-1}$. Selection of *H. pylori* mutants
798 was performed using kanamycin 20 $\mu g.ml^{-1}$, Streptomycin 10$\mu g.ml^{-1}$, Apramycin
799 10$\mu g.ml^{-1}$ or chloramphenicol 8 $\mu g.ml^{-1}$. For liquid cultures, we used Brain Heart
800 Infusion (BHI) broth (Oxoïd) supplemented with 10% Fetal Calf Serum (FCS) (Eurobio),
801 the antibiotics-antifungal cocktail and the selective antibiotic when necessary. *H. pylori*
802 cells were grown at 37°C under microaerophilic atmosphere conditions (6% O_2, 10%
803 CO_2, 84% N_2) using an Anoxomat (MART Microbiology) atmosphere generator. When
804 indicated, 1mM of isopropyl ß-D-1-thiogalactopyranoside (IPTG, EuroMedex) was
805 added to agarose pads or culture media.

806

807 ***Molecular techniques***

808 Molecular biology experiments were performed according to standard procedures
809 and the supplier (Fermentas) recommendations. NucleoBond Xtra Midi Kit (Macherey-
810 Nagel) and QIAamp DNA Mini Kit (Qiagen) were used for plasmid preparations and *H.*
811 *pylori* genomic DNA extractions, respectively. PCR were performed either with Taq
812 Core DNA polymerase (MP Biomedicals), or with Phusion Hot Start DNA polymerase
813 (Finnzymes) when the product required high fidelity polymerase. The pGEM-T easy

814 vector systems (Promega) was used to construct, in *E. coli*, the suicide plasmids that
815 served for markerless deletions of TA systems in *H. pylori*.
816
817 ***Construction of H. pylori strains carrying mutations or plasmids***
818 Mutations of *H. pylori* were introduced into strain B128 either WT or a streptomycin
819 resistant variant B128 *rpsL1* for markerless mutagenesis (31, 56). Chromosomal
820 deletions of the *AapA1/*IsoA1 locus, of the *flaA* gene, or of the different class A TA loci
821 were performed either by insertion of a selectable antibiotic resistance marker to
822 disrupt or replace the gene of interest or when necessary, by the markerless counter-
823 selected mutagenesis strategy (31, 56). Plasmids were derived from the pILL2157 *E.*
824 *coli/H. pylori* shuttle vector that contains an IPTG-inducible promoter (27). Deletions
825 were introduced by allelic exchange using suicide plasmids (see suppl **Table S3**) or
826 PCR fragments. Introduction of plasmids and construction of *H. pylori* mutants were
827 obtained by natural transformation and selection with the corresponding antibiotic as
828 described previously (31). PCR and sequencing of the regions of interest were used
829 to validate the introduction of plasmids, deletion of genes of interest and correct
830 insertion of fusions. Primers used for these constructs or their validation are listed in
831 Suppl **Table S4.**
832
833 **Fluorescence Microscopy**
834 Fluorescence microscopy was performed with an Axio Observer microscope (Zeiss)
835 equipped with an Axiocam camera under an X100 magnification. Acquisition images
836 was performed using the axiovision software. Images were cropped and adjusted using
837 ImageJ v2.0.0 software. Cells were quantified and assigned to helical or coccoid
838 categories based on phase contrast images by using the MicrobeJ plugin of ImageJ
839 (28) with the following parameters: (i) helical cells had an area of more than 0.7 μm^2,

840 a length between 1 and 5 μm, a width between 0.4 and 1 μm and a circularity of less
841 than 0.8, and (ii) coccoid cells had an area between 1 and 2 μm^2, a width between 0.4
842 and 1.7 μm and a circularity greater than 0.7.

843 *H. pylori* B128 strains were grown in BHI medium with chloramphenicol (8 µg/ml) to
844 maintain the plasmids. 1 mM IPTG was added to the culture and samples were taken
845 at different time-points, concentrated by 2 min centrifugation at 3000 x g and washed
846 twice with PBS buffer. Cells were immobilized using 2% (wt/vol) agarose pads
847 containing PBS before being imaged. In **Fig. 1C**, cell membranes were stained with
848 4% FM4-64 (Thermofisher Scientific). In **Fig. 2B**, cell membranes were stained with
849 0.01 mM TMA-DPH (1-(4-trimethylammoniumphenyl)-6-phenyl-1,3,5-hexatriene p-
850 toluenesulfonate, Euromedex).

851

852 **Flow cytometry for proton motive force (PMF) measurement**

853 *H. pylori* strains were grown in triplicate for 16h and then treated or not with 1 mM
854 IPTG. Samples were taken at 0, 8 and 24h post-induction and 10^7 live cells per
855 experimental condition were washed and stained with 25 nM MitoTracker® Red
856 CMXRos (Invitrogen), a PMF-sensitive dye. As a control for PMF depletion, pA1* cells
857 were treated with 500µM of the protonophore TCS (3,3',4',5-Tetrachlorosalicylanilide;
858 Fisher scientific). The fluorescent signal from at least 100,000 individual bacteria per
859 condition was measured by flow cytometry with a MCSQuant® VYB analyzer (Miltenyi
860 Biotec) (Y2 channel, λ_{ex}=561 nm and λ_{em}=605-625 nm) after calibration. The
861 experiment was performed three times. Data were analyzed with FlowJo V10.

862

863 **Fractionation and Immunoblotting**

864 The protocol of *H. pylori* fractionation was adapted from (57). *H. pylori* strains were

865 grown in the absence or presence of 1mM IPTG. When cultures reached OD_{600} 0.8,
866 cells were harvested by centrifugation, washed twice in phosphate-buffered saline
867 medium (PBS) prior to their disruption by sonication in Buffer 1, 10mM Tris-HCl, pH
868 7.5 containing 5mM ß-mercaptoethanol and proteases inhibitors (cOmplete™, EDTA-
869 free Protease Inhibitor Cocktail, Roche). Cell debris were removed by centrifugation
870 (10 min, 16,000 x *g*, 4°C) and supernatants containing the soluble extract and
871 membrane fractions were collected as total extracts. Samples of total extracts were
872 frozen and the remaining supernatants were subjected to ultracentrifugation (125,000
873 x *g*, 45 min, 4°C). Samples from the supernatant containing the cytoplasm and
874 periplasm were collected and frozen while pellets containing total membranes were
875 resuspended in buffer 1 supplemented with 1% N-lauroylsarcosine (buffer 2) prior to
876 being ultracentrifuged (125,000 x *g*, 45 min, 4°C). Samples of inner membrane
877 fractions from supernatants were frozen. Outer membrane pellets were washed twice
878 in buffer 2 to avoid inner membrane fractions contamination prior to freezing. For each
879 cellular compartment, equal cellular amounts were loaded and separated on a 4-20%
880 Mini-Protean TGX precast protein gel (BioRad) and subsequently electrotransferred
881 on a polyvinylidene difluoride (PVDF) membrane (Biorad). The control *H. pylori*
882 proteins PPB2, AlpA and AmiE and NikR as well as the fusion protein A1-GFP were
883 detected with rabbit polyclonal antibodies α-PBP2 (58), α-AlpA (57), α-AmiE (59) and
884 α-NikR (60); with goat anti-GFP-HRP antibody (Abcam) at the respective dilutions of
885 1:2,000, 1:1,000, 1:100, 1:5,000 and 1:5,000. Goat anti-rabbit IgG-HRP (Santa Cruz)
886 was used as secondary antibody (1:10,000 dilution) and the detection was achieved
887 with the ECL reagent (ThermoFisher Scientific).
888
889 **ATP extraction and assay**

890 Exponentially growing *H. pylori* cells (6h of culture) and stationary growing cells
891 (16h) were harvested by centrifugation at room temperature for 4 min at 5000*g*.
892 Metabolites from the resulting cell pellets were extracted immediately using 300µL of
893 a solvent mixture of Acetonitrile/Methanol/H_2O (40/40/20) for 15min at 4°C and 10min
894 at 95°C. Mixtures were subsequently spun in a microfuge for 5 min at maximum speed
895 and 4°C to separate insoluble materials from the extracted metabolites. The resulting
896 pellets were then re-extracted twice with 200 µL of solvent at 4°C. The supernatants
897 were pooled to yield 700 µL of final extract. Metabolites were lyophilized and
898 subsequently diluted in water for ATP assays. ATP content was determined by a
899 luciferase-based ATP bioluminescence assay kit (BacTiter-Glo™ Microbial cell viability
900 assay, Promega). Luminescence values were determined using a 10 sec RLU signal
901 integration time and measured using a Centro XS^3 LB960 Luminometer (Berthold
902 Technologies). ATP concentrations were calculated based on values determined using
903 serial dilutions of known amounts of ATP and expressed as a function of the OD_{600nm}
904 of the corresponding culture.
905
906 **Cryo-electron microscopy**
907 Four µL of *H. pylori* bacteria were spotted on glow-discharged lacey grids (S166-3,
908 EMS) or Quantifoil R2/2 (Quantifoil, Germany). The samples were cryo-fixed by plunge
909 freezing at -180°C in liquid ethane using a Leica EMGP (Leica, Austria). Grids were
910 observed at 200kV with a Tecnai F20 (Thermo Fisher Scientific). Images were
911 acquired under low-dose conditions using the software EPU (Thermo Fisher Scientific)
912 and a direct detector Falcon II (Thermo Fisher Scientific).
913
914 **Time-lapse microscopy**

915 Confocal analysis of live cells was performed as previously described (61). Twenty
916 µL of exponentially grown bacteria (10^5 cells) suspended in BHI with or without 1mM
917 IPTG were deposited on 35mm glass bottom Petri dishes. The suspension was
918 covered with BHI medium in 1.5% low melting agarose supplemented with
919 Chloramphenicol (8µg/µl) with or without IPTG (1mM). Live-cell imaging was
920 performed with a Nikon A1R confocal laser scanning microscope system attached to
921 an inverted ECLIPSE Ti (Nikon Corp., Tokyo, Japan) and equipped with an
922 environmental chamber allowing the control of temperature (37°C), humidity (90%) and
923 gas mixture (10% CO_2, 3% O_2). GFP fluorescence images were captured through a
924 Plan APO 60X objective (NA: 1.40) by using optimal spatial resolution settings. The
925 cytoplasm compartment volume was defined by using GFP staining (excitation with
926 488 nm laser, emission collected with an 500/50 nm filter set). Image captions were
927 performed every 10min during 10h. Image treatment and analysis were performed
928 using NIS elements (Nikon Corp., Tokyo, Japan), and ImageJ and MicrobeJ software
929 (28).
930
931 **ß-galactosidase activity assays**
932 B128Δ*AapA1-IsoA1::PaapA1-lacZ-Kan* and B128Δ*AapA1-IsoA1::PIsoA1-lacZ-Kan*
933 strains were grown to OD_{600nm} 0.3 in BHI liquid medium, then divided into two samples,
934 one of them being submitted to stress conditions during 6h with 5, 50 and 500 µM
935 paraquat (Sigma), 0.03 and 0.3% hydrogen peroxide (Sigma), 20 and 200 mM $NiCl_2$
936 (Sigma), acidic pH, antibiotics with 0.1 and 1 mg/mL tetracycline, or 0.05 and 0.5 mg/ml
937 rifampicin. Then 0.5ml samples were taken, washed twice with 1X PBS (Phosphate
938 Buffered Saline) and further permeabilized with 100µL Chloroform and 50µl SDS 0.1%
939 in Z buffer containing 70mM Na_2HPO_4, 30mM NaH_2PO_4, 1mM $MgSO_4$ and 0.2mM
940 $MnSO_4$ (62). Samples were briefly vortexed and incubated at 28°C for 2 min. The ß-

941 galactosidase assay was started by adding 0.1mL ONPG (ortho-nitrophenyl-β-
942 galactoside, ThermoFischer) at 4mg/ml and stopped by the addition of 0.5mL 1M
943 Na_2CO_3 when sufficient yellow color was reached. The ß-galactosidase activity is
944 expressed in Miller units (62) and represented in **Fig. 5** and **S6** as percentage of
945 activities relative to the control activity with the corresponding strains not exposed to
946 stress and was calculated from 3 independent experiments performed in duplicates.
947

948 **Total RNA extraction and Northern blotting**

949 Total RNAs were extracted from 10 mL *H. pylori* cultures (OD_{600} 0.5 -0.9) exposed
950 or not to 1% H_2O_2 using the NucleoSpin miRNA kit (Macherey Nagel) at different time
951 points after 80 µg/mL rifampicin addition (to stop transcription). For Northern blotting,
952 5 µg of total RNA were separated on 10% Mini protean TBE Urea gel (Biorad) and
953 transferred to Hybond N+ (Amersham Biosciences) membrane using a Trans-Blot
954 Turbo system (Biorad). A denaturated DNA marker was used for size estimation.
955 Transferred RNA was fixed to the membrane by UV irradiation for 2 min. The
956 membrane was blocked for 45 min at 42°C with ULTRAhyb Hybridization Buffer
957 (Ambion), then 20 µl of 5'-labeled ($\gamma^{32}P$) oligodeoxynucleotides (**Table S4**) were added
958 and the membrane was further incubated overnight at the same temperature. After
959 three washes for 10 min at 65°C with 2x SSC 0.2 % SDS, the membrane was exposed
960 to a phosphorimager screen (KODAK) and scanned with FLA-9000 Phospho Imager
961 (Fujifilm).
962

963 **Peptidoglycan extraction and Muropeptides analysis by HPLC/HRMS (high**
964 **resolution mass spectrometry)**

965 Samples corresponding to 2 mL of culture at OD_{600nm} 10 of *H. pylori* were taken and
966 chilled in an ice-ethanol bath, each condition was prepared in triplicates. The samples
967 were B128 WT strain in exponential phase (24h culture); stationary phase (36h
968 culture); after 72h culture ("aging coccoids"). To examine the effect of the A1 toxin, we
969 performed a culture of 16 h, added IPTG and then took samples of the following strains:
970 B128 ΔaapA1-IsoA1 + pA1 strain after 8h of induction (equivalent to 24h of total culture
971 time) or 24 h of induction (equivalent to 36h); and as a negative control, of strain B128
972 ΔaapA1-IsoA1 + pA1* after 8h and 24 h of induction (total 24h and 36h, respectively).
973 Crude murein sacculi were immediately extracted in boiling sodium dodecyl sulfate
974 (SDS 4% final) (63). The resulting purified peptidoglycan was digested overnight at
975 37°C in 12.5 mM sodium phosphate buffer (pH 5.6) supplemented with 100 UI of
976 mutanolysin from *Streptomyces globisporus* ATCC 21553 (Sigma). The reaction was
977 stopped by heat inactivation of the enzyme and insoluble material was removed by
978 centrifugation. Soluble muropeptides were then reduced with sodium borohydride in
979 borate buffer (pH 9). After centrifugation, reduced muropeptides were diluted 20-fold
980 in water-formic acid 0.1% (v/v; solvent A). HPLC/HRMS (High Performance Liquid
981 Chromatography/High Resolution Mass Spectrometry) was performed on an Ultimate
982 3000 UHPLC (Ultra High-Performance Liquid Chromatography) system coupled to a
983 quadrupole-Orbitrap mass spectrometer (Q-Exactive Focus, Thermo Fisher Scientific).
984 Muropeptides were separated on an Hypersil Gold aQ analytical column (1.9 µm,
985 2.1x150 mm) at 200 µL/min, column temperature at 50°C. Applied linear gradient from
986 0 to 12.5% acetonitrile + 0,1% (v/v) formic acid (solvent B), followed by increasing to
987 20% B at 25 min for 5 min, hold 20% B for min and additional 10 min with 100% A for
988 column re-equilibration. Eluted muropeptides were introduced into Q-Exactive
989 instrument, operating in positive ion mode, and then were analyzed in the data-
990 dependent acquisition mode (FullMSddMS2). The identification of muropeptides was

991 performed after precursor ion fragmentation (MS2 analysis). Data were then
992 processed with the software TraceFinder 3.3 (Thermo Fisher Scientific) for peak areas
993 determination, the relative abundance of muropeptides in each sample was calculated
994 according to Glauner *et al.* (30).
995
996 **Statistical analysis**
997 The Student's t test was used to determine significance of the means of the data for
998 all the experiments except for the Northern blots. Error bars represent the standard
999 deviation, with * ($P < 0.05$), ** ($P < 0.01$), *** ($P < 0.001$), **** ($P < 0.0001$) indicating
1000 that the mean values are significantly different and NS that they are not significantly
1001 different ($P > 0.05$). SEM corresponds to standard error of the mean. The two-way
1002 ANOVA multiple comparisons test was used to compare Northern blots bands
1003 intensities under different conditions.
1004

Figure 1

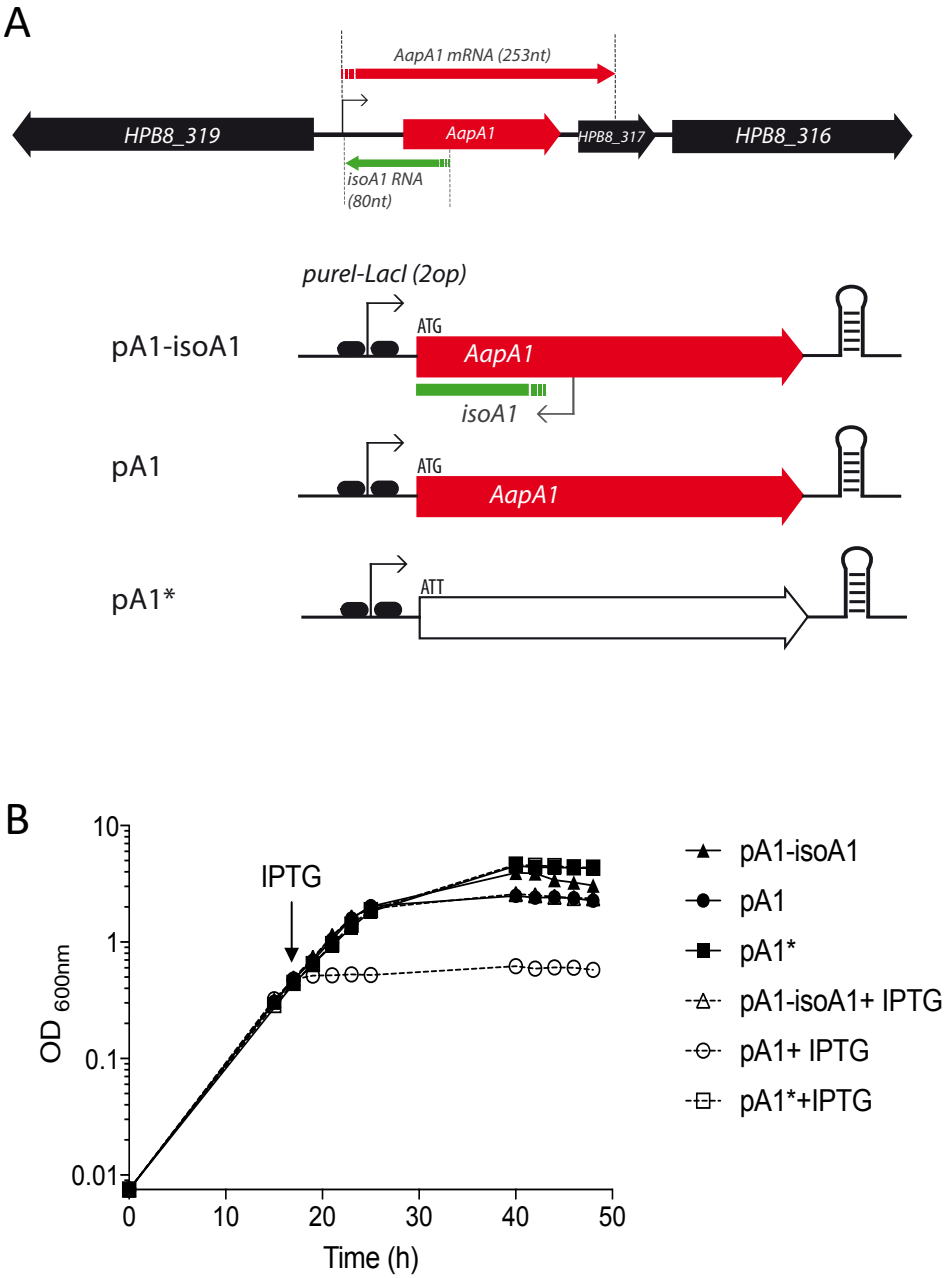
A
AapA1 mRNA (253nt)
HPB8_319
AapA1
HPB8_317
HPB8_316
isoA1 RNA
(80nt)
purel-LacI (2op)
pA1-isoA1
ATG
AapA1
isoA1
pA1
ATG
AapA1
pA1*
ATT
B
IPTG
OD 600nm
Time (h)
pA1-isoA1
pA1
pA1*
pA1-isoA1+ IPTG
pA1+ IPTG
pA1*+IPTG

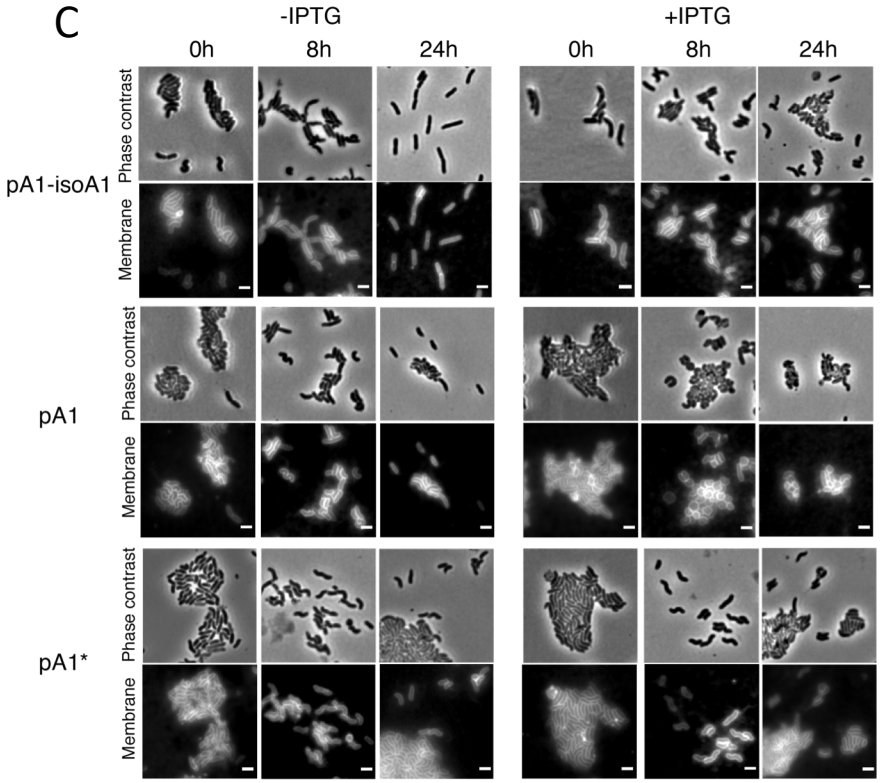
C
-IPTG
+IPTG
0h
8h
24h
pA1-isoA1
pA1
pA1*
Phase contrast
Membrane

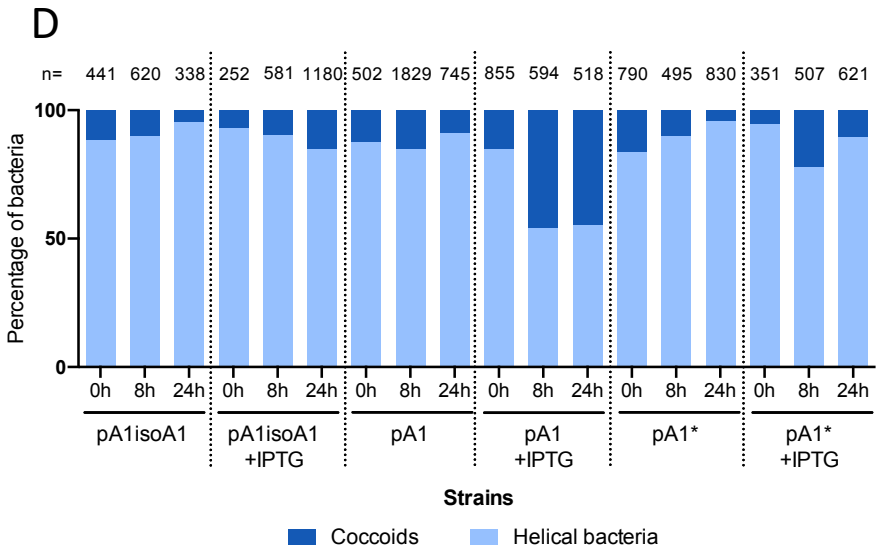
D
n= 441 620 338 252 581 1180 502 1829 745 855 594 518 790 495 830 351 507 621
Percentage of bacteria
0h 8h 24h
pA1isoA1
pA1isoA1 +IPTG
pA1
pA1 +IPTG
pA1*
pA1* +IPTG
Strains
Coccoids
Helical bacteria

Figure 2

A

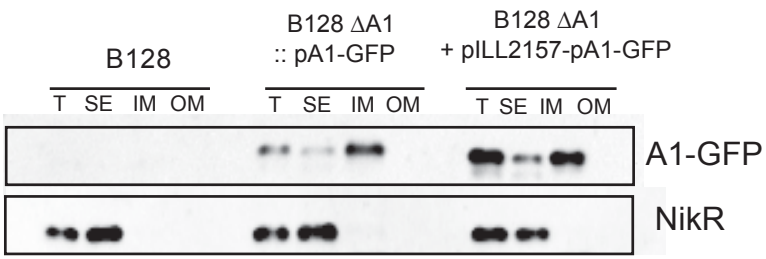

B

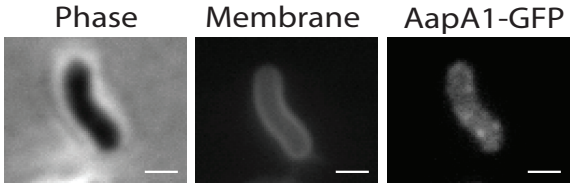

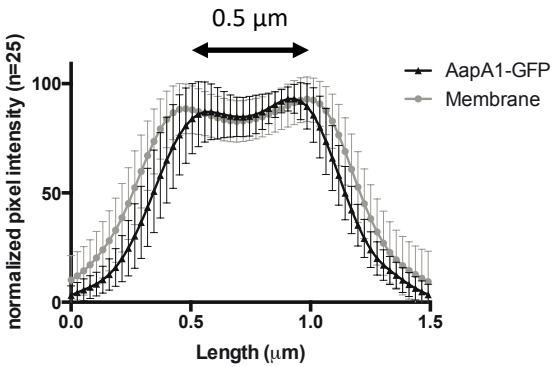

C

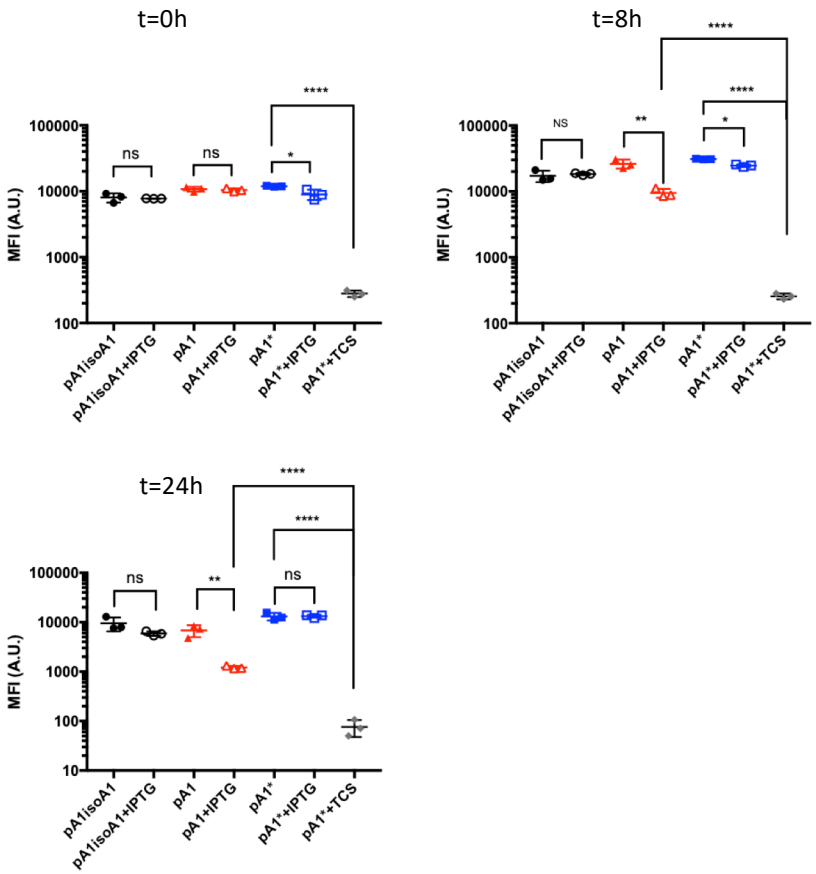

D

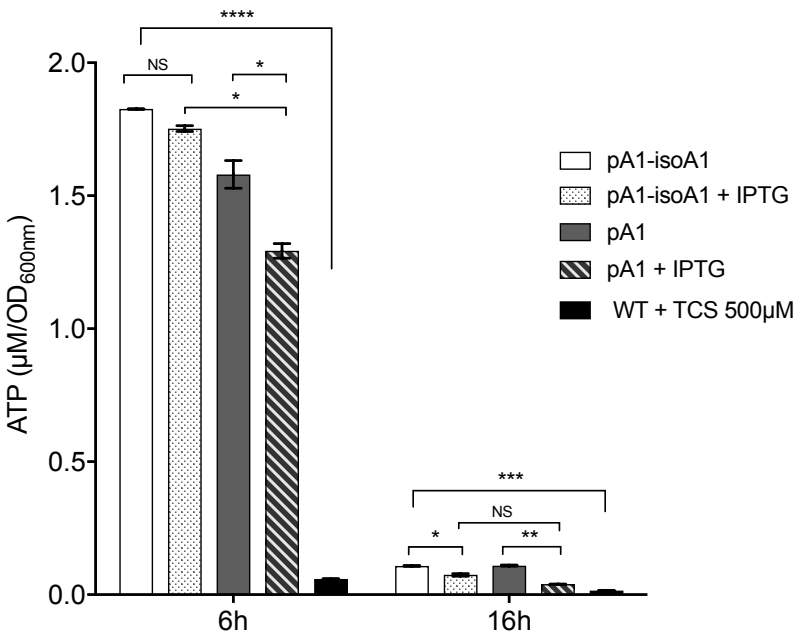

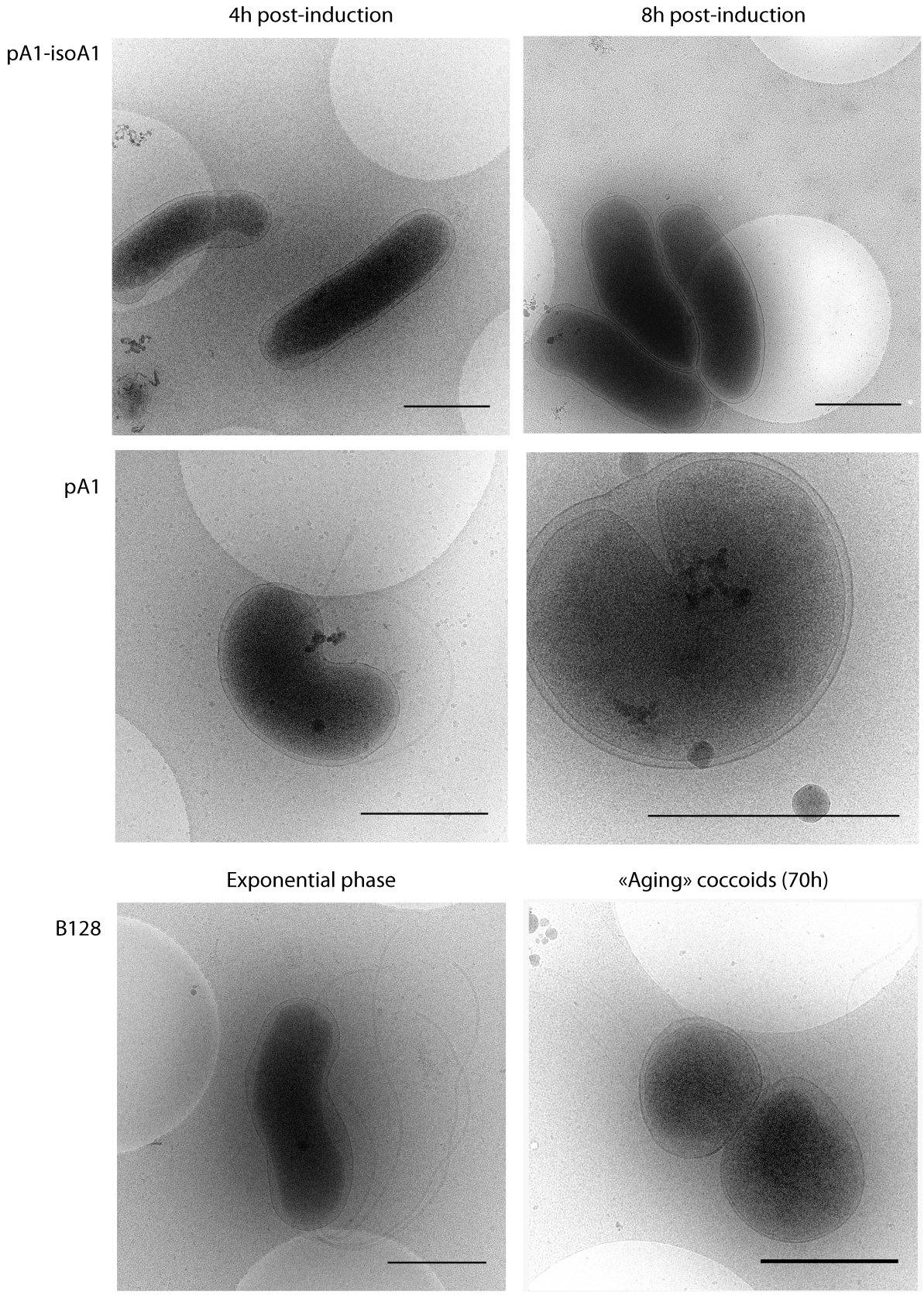
4h post-induction
8h post-induction
pA1-isoA1
pA1
Exponential phase
«Aging» coccoids (70h)
B128

Figure 4

A

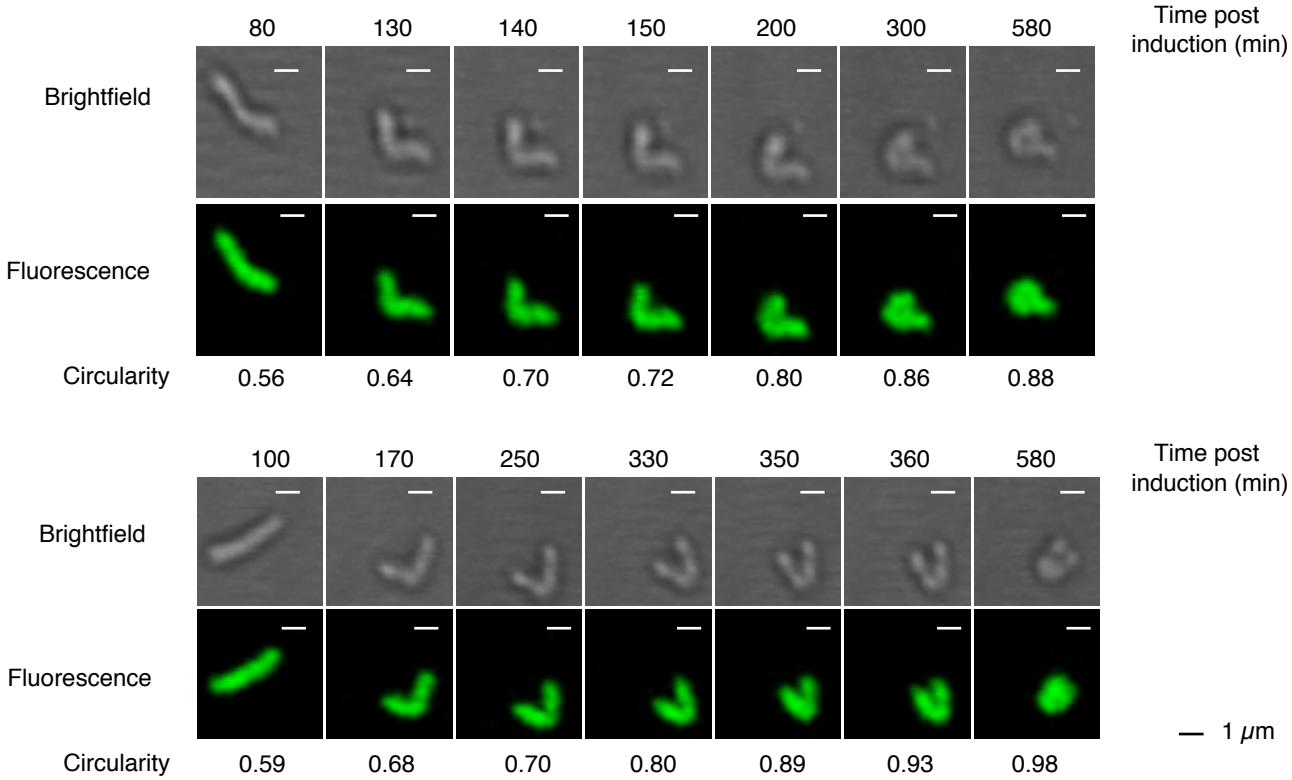
80
130
140
150
200
300
580
Time post induction (min)
Brightfield
Fluorescence
Circularity
0.56
0.64
0.70
0.72
0.80
0.86
0.88
100
170
250
330
350
360
580
Time post induction (min)
Brightfield
Fluorescence
Circularity
0.59
0.68
0.70
0.80
0.89
0.93
0.98
1 μm

B

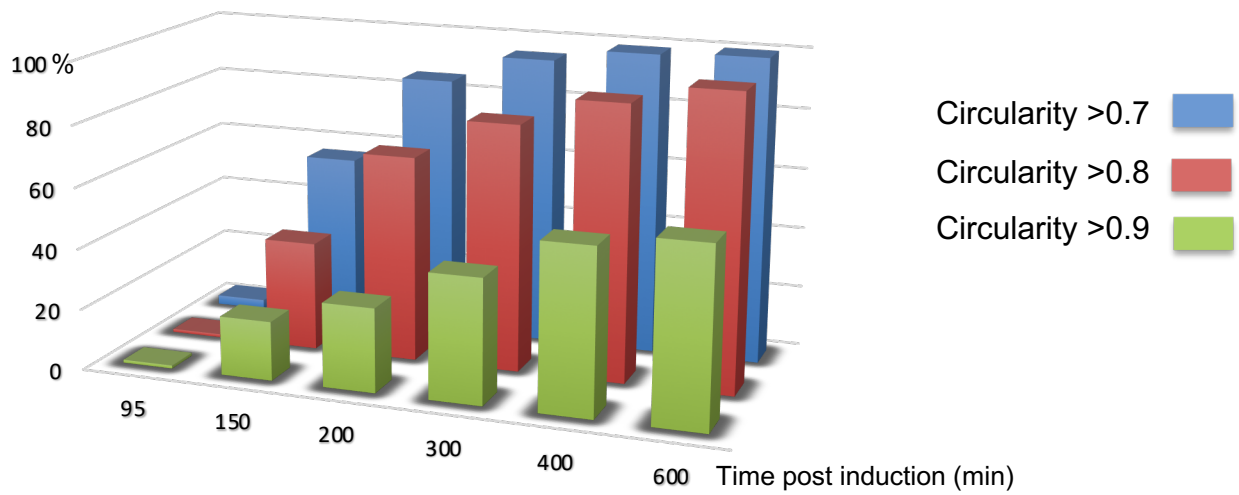
100 %
80
60
40
20
0
95
150
200
300
400
600
Time post induction (min)
Circularity >0.7
Circularity >0.8
Circularity >0.9

Figure 5

A.

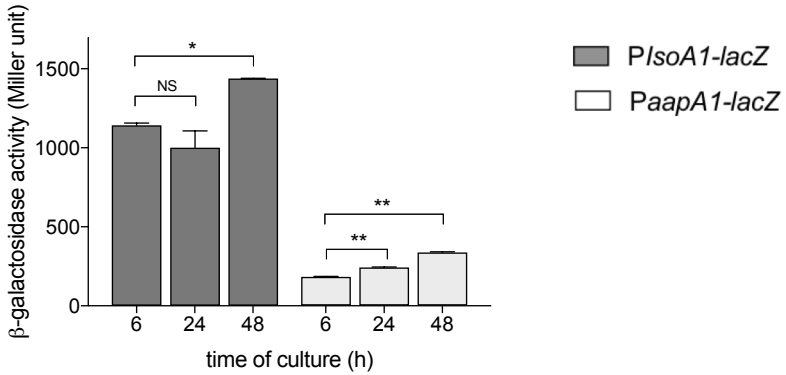

B.

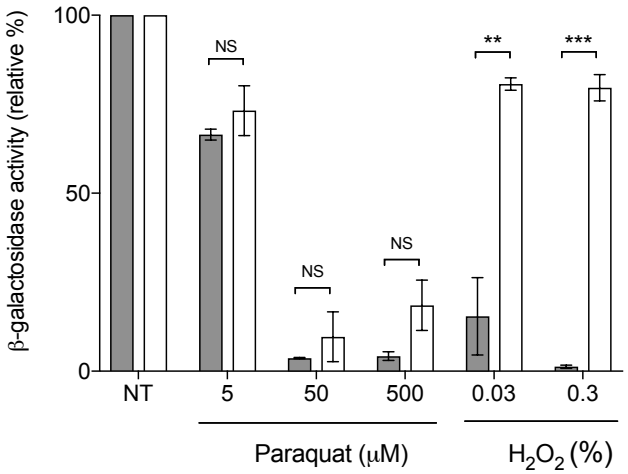

C.

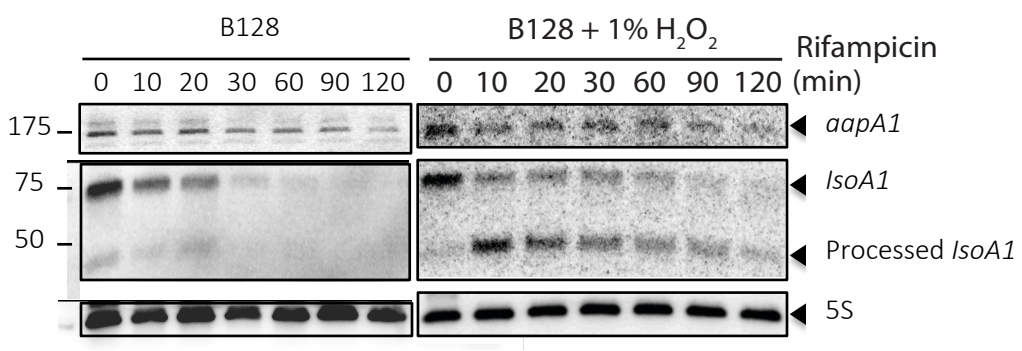
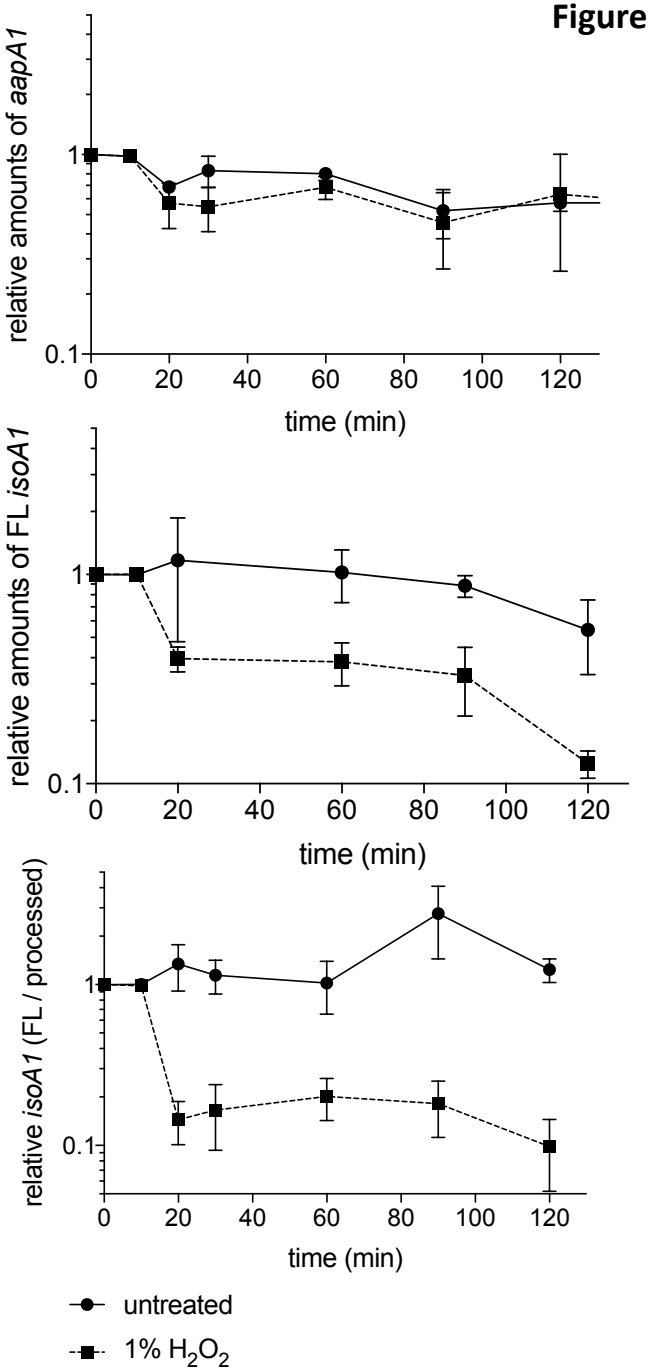
D.